Article

Cell

TACAN Is an Ion Channel Involved in Sensing Mechanical Pain

Graphical Abstract

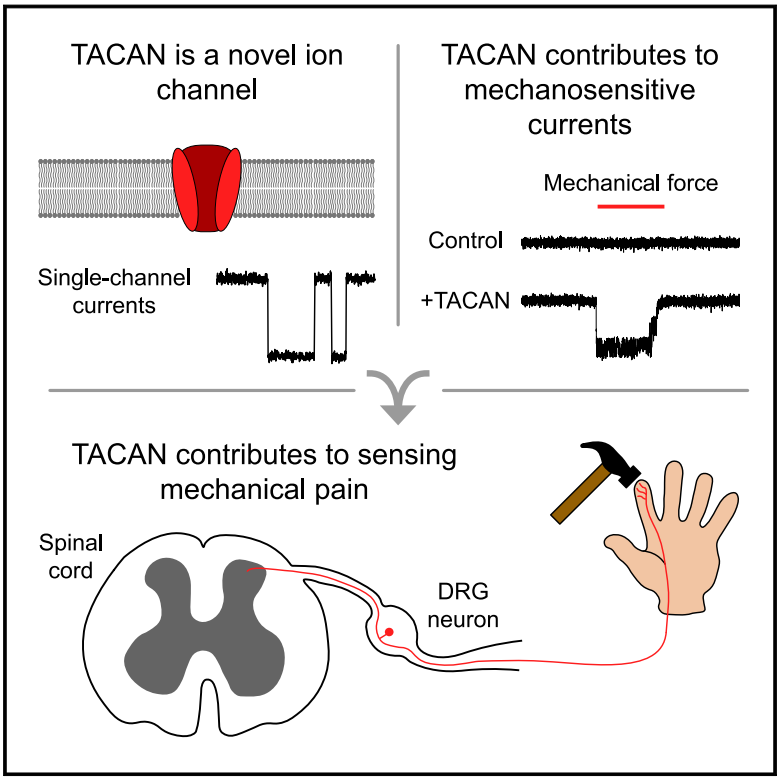

Authors

Lou Beaulieu-Laroche, Marine Christin, Annmarie Donoghue, ..., Kate Poole, Emmanuel Bourinet, Reza Sharif-Naeini

Correspondence

reza.sharif@mcgill.ca

In Brief

TACAN is identified as an ion channel that contributes to mechanosensitive currents in nociceptors and detecting mechanical pain stimuli.

Highlights

- Identification of TACAN as an ion channel
- TACAN contributes to mechanosensitive currents in nociceptors
- TACAN contributes to sensing mechanical pain

Beaulieu-Laroche et al., 2020, Cell *180*, 956–967
March 5, 2020
https://doi.org/10.1016/j.cell.2020.01.033

CellPress

Cell

Article

TACAN Is an Ion Channel Involved in Sensing Mechanical Pain

Lou Beaulieu-Laroche,[1,2,15,16] Marine Christin,[1,2,16] Annmarie Donoghue,[3] Francina Agosti,[4] Noosha Yousefpour,[2,5] Hugues Petitjean,[1,2] Albena Davidova,[1,2] Craig Stanton,[1,2] Uzair Khan,[1] Connor Dietz,[1] Elise Faure,[7] Tarheen Fatima,[1,2] Amanda MacPherson,[1] Stephanie Mouchbahani-Constance,[1,2] Daniel G. Bisson,[8,9] Lisbet Haglund,[8,9] Jean A. Ouellet,[9,10] Laura S. Stone,[2,5,6] Jonathan Samson,[11] Mary-Jo Smith,[12] Kjetil Ask,[13] Alfredo Ribeiro-da-Silva,[2,5] Rikard Blunck,[3,7] Kate Poole,[14] Emmanuel Bourinet,[4] and Reza Sharif-Naeini[1,2,17,*]

[1]Department of Physiology and Cell Information Systems, McGill University, Montreal, QC, Canada
[2]Alan Edwards Center for Research on Pain, McGill University, Montreal, QC, Canada
[3]Department of Physics, Université de Montréal, Montreal, QC, Canada
[4]Institut de Génomique Fonctionnelle, Université de Montpellier, CNRS, INSERM, Montpellier, France
[5]Department of Pharmacology and Therapeutics, McGill University, Montreal, QC, Canada
[6]Faculty of Dentistry, McGill University, Montreal, QC, Canada
[7]Department of Pharmacology and Physiology, Université de Montréal, Montreal, QC, Canada
[8]Orthopaedic Research Laboratory, Division of Orthopaedic Surgery, McGill University, Montreal, QC, Canada
[9]Shriners' Hospital for Children, Montreal, QC, Canada
[10]McGill Scoliosis and Spine Research Group, McGill University, Montreal, QC, Canada
[11]Advanced Cell Diagnostics, Newark, Toronto, ON, Canada
[12]Department of Pathology and Molecular Medicine, McMaster Immunology Research Centre, McMaster University, Hamilton, ON, Canada
[13]Department of Medicine, Firestone Institute for Respiratory Health and McMaster Immunology Research Centre, McMaster University, Hamilton, ON, Canada
[14]EMBL Australia Node in Single Molecule Science, School of Medical Sciences, University of New South Wales, Sydney, NSW, Australia
[15]Present address: Department of Brain and Cognitive Sciences and McGovern Institute for Brain Research, Massachusetts Institute of Technology, Cambridge, MA, USA
[16]These authors contributed equally
[17]Lead Contact
*Correspondence: reza.sharif@mcgill.ca
https://doi.org/10.1016/j.cell.2020.01.033

SUMMARY

Mechanotransduction, the conversion of mechanical stimuli into electrical signals, is a fundamental process underlying essential physiological functions such as touch and pain sensing, hearing, and proprioception. Although the mechanisms for some of these functions have been identified, the molecules essential to the sense of pain have remained elusive. Here we report identification of TACAN (Tmem120A), an ion channel involved in sensing mechanical pain. TACAN is expressed in a subset of nociceptors, and its heterologous expression increases mechanically evoked currents in cell lines. Purification and reconstitution of TACAN in synthetic lipids generates a functional ion channel. Finally, a nociceptor-specific inducible knockout of TACAN decreases the mechanosensitivity of nociceptors and reduces behavioral responses to painful mechanical stimuli but not to thermal or touch stimuli. We propose that TACAN is an ion channel that contributes to sensing mechanical pain.

INTRODUCTION

The sensations of touch and pain are essential for our interactions with the environment. They rely on a cellular phenomenon called mechanotransduction, during which mechanical forces are converted into electrical signals. This vital process underlies several physiological functions, such as hearing, touch, pain, and proprioception (Boyer et al., 2011; Chalfie, 2009; Li et al., 2012; Woo et al., 2015), as well as the myogenic tone of resistance arteries (Sharif-Naeini et al., 2009), fluid homeostasis and the sensation of thirst (Bourque, 2008; Zaelzer et al., 2015), and flow sensing in kidney tubules (Peyronnet et al., 2012). Many of these processes require mechanotransduction at the micro- to millisecond scale, suggesting that the transducers are mechanosensitive ion channels (MSCs). The requirement for MSCs in these processes is confirmed by the recent discovery of genes responsible for the senses of touch (Ranade et al., 2014b), hearing (Pan et al., 2013), and proprioception (Boyer et al., 2011; Hong et al., 2016; Woo et al., 2015). However, the genes responsible for the most unpleasant type of mechanotransduction, the sense of pain, remain elusive. Here we report identification of an ion channel for pain sensing. We find that TACAN contributes to mechanosensitive currents in nociceptors and mechanical pain sensing in mice.

RESULTS

TACAN Is a Candidate Ion Channel with Potential Mechanosensitive Properties Found in Nociceptors

A previous proteomic screen of membrane proteins involved in mechanotransduction in smooth muscle cells generated a list

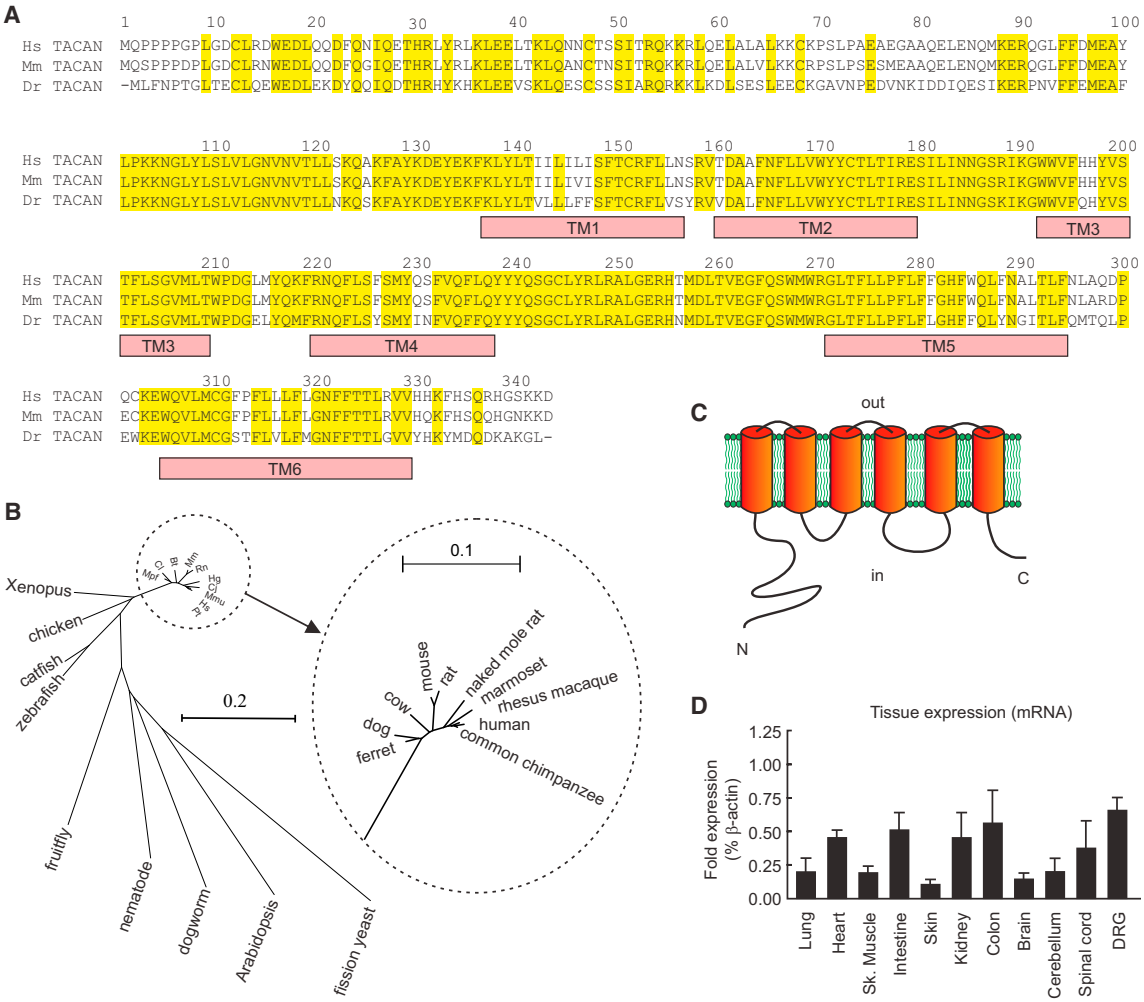

Figure 1. Analysis of TACAN Amino Acid Sequence, Phylogenetic Tree, and Predicted Membrane Topology

(A) Comparison of the amino acid sequences for TACAN from human (Hs), mouse (Mm), and zebrafish (Dr). Amino acid residues are numbered from the first methionine of Hs TACAN. Conserved residues are highlighted in yellow, and predicted transmembrane (TM1–TM6) segments are indicated by orange boxes, as predicted by the CCTOP server.

(B) Unrooted phylogenetic tree showing the sequence relationship of TACAN in different species. Alignments were generated by Clustal-Omega, and the phylogenetic tree was generated using Unrooted (http://pbil.univ-lyon1.fr/software/unrooted.html). Scale: number of substitutions per position.

(C) Predicted membrane topology of TACAN.

(D) TACAN mRNA expression in different tissues.

See also Table S1.

of over 70 candidates (Sharif-Naeini et al., 2009), including some transmembrane proteins of unknown function. One of these candidates, which we named TACAN (for "movement" in Farsi), also known as TMEM120A, NET29, or TMPIT, is highly conserved (>70% homology) in vertebrates, and conserved at lower levels in invertebrates (Figures 1A and 1B; Table S1). The predicted membrane topology (constrained consensus topology [CCTOP]) suggests that TACAN has 6 transmembrane domains with internal amino and carboxyl termini (Figure 1C). Tissue expression analysis revealed that TACAN is expressed in several tissues (Figure 1D), with higher expression in the heart, kidneys, colon, and sensory neurons of the dorsal root ganglia (DRGs). Given the role of DRG neurons in the senses of touch and pain, we examined whether TACAN expression was restricted to specific subsets of mouse sensory neurons. *In situ* hybridization experiments (Figure 2A) demonstrated the presence of TACAN mRNA in DRG neurons. Analysis of the cross-sectional area distribution revealed that TACAN expression is present in small- to medium-diameter neurons (Figure 2B), suggesting that TACAN could be expressed in nociceptors. A similar pattern of distribution was evident when examining TACAN expression in human DRGs, with large co-expression in nociceptors (Figure S1). To examine the subset of sensory neurons expressing TACAN, we generated a rabbit anti-TACAN antibody (Figure S2). Our data indicate that TACAN is highly expressed in mouse non-peptidergic nociceptors, based on colabeling with markers such as

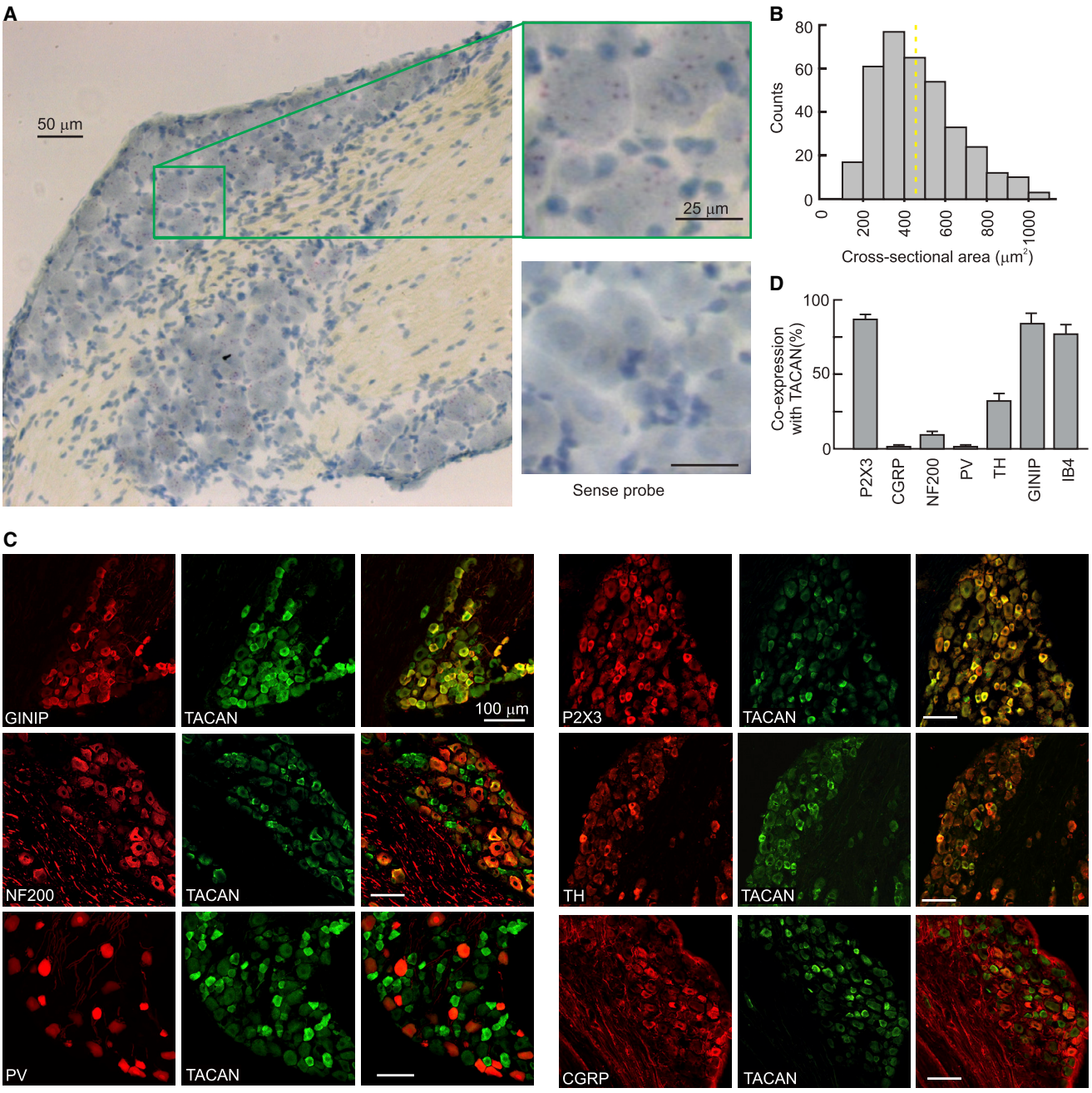

Figure 2. TACAN Is Expressed in Nociceptors

(A) *In situ* hybridization examining the presence of TACAN in mouse DRG sections. Top right panel: magnification of the box in the left panel, with the TACAN probe. Bottom right panel: magnification of a DRG section probed with a sense (control) probe.

(B) Cross-sectional area distribution of TACAN mRNA-positive neurons. The yellow dashed line represents the mean of all DRG neurons analyzed.

(C) Double immunostaining to determine colocalization of TACAN with markers of myelinated afferents (Neurofilament 200 [NF200]), peptidergic (CGRP) and non-peptidergic (P2X3) nociceptors, C-type low-threshold mechanoreceptors (C-LTMRs; tyrosine hydroxylase [TH]), and GINIP (C-LTMRs and non-peptidergic nociceptors). Colocalization with proprioceptors was done by staining DRG sections of *Pvalb:cre; tdTom* mice with the TACAN antibody.

(D) Percentage (± SEM) of marker-immunoreactive neurons that co-express TACAN.

See also Figures S1 and S2.

P2X3, GINIP, and IB4 (Figures 2C and 2D). Co-labeling was low with markers of myelinated neurons (NF200), peptidergic nociceptors (CGRP), or proprioceptors (parvalbumin). Tyrosine hydroxylase (TH), a marker of low-threshold C-fibers, was found in about a third of TACAN-positive sensory neurons. However, over 80% of TH-positive neurons (82.7% + 3.9%) were positive

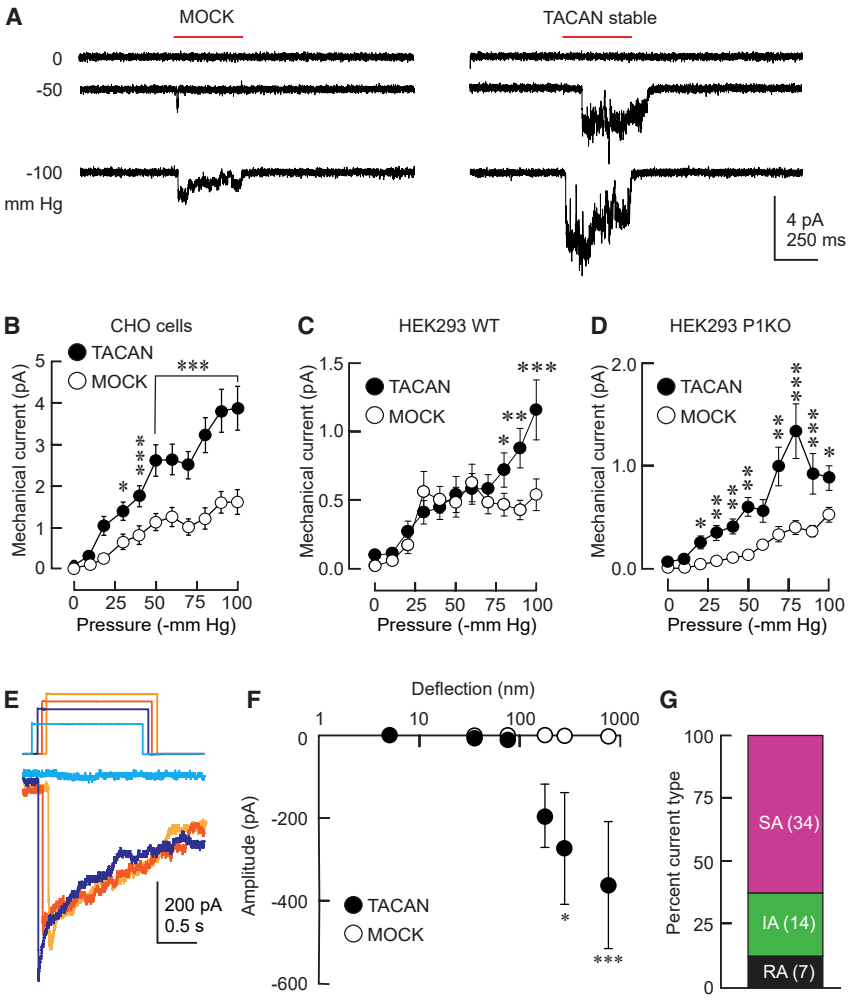

Figure 3. TACAN Expression Increases Mechanically Evoked Currents in Heterologous Systems

(A) Representative cell-attached current traces elicited by mechanical stimuli (red bar) in CHO cells stably expressing TACAN (right) or mock (left).

(B) Mean (± SEM) mechanically evoked currents (right panel, V_{hold} = −80 mV) in stable CHO cells expressing mock (n = 58) or TACAN (n = 61). *p < 0.05, ***p < 0.001. Asterisks indicate significant difference from the mock group (two-way ANOVA with Tukey post hoc test).

(C) Mean (± SEM) mechanically evoked currents (V_{hold} = −80 mV) in HEK293 cells expressing mock (n = 79) or TACAN (n = 57).

(D) Mean (± SEM) mechanically evoked currents (V_{hold} = −100 mV) in HEK293 Piezo1 knockout cells (P1KO) cells expressing mock (n = 68) or TACAN (n = 67).

(C and D) *p < 0.05, **p < 0.01, ***p < 0.001. Asterisks indicate significant difference from the mock group (two-way ANOVA with Tukey post hoc test).

(E) Representative whole-cell current traces elicited by mechanical stimulation of the pillars of subjacent P1KO cells transiently transfected with TACAN. The extent of pillar deflection is indicated by colors, with blue, purple, orange, and yellow traces corresponding to deflections of 134, 223, 234, and 304 nm, respectively.

(F) Mean (± SEM) mechanically evoked whole-cell currents (V_{hold} = −60 mV) in P1KO cells transfected with TACAN (n = 6) or mock (n = 9). *p < 0.05, ***p < 0.001, using two-way ANOVA with Sidak's multiple comparison test.

(G) Prevalence of the three types of adaptation kinetics (rapid, intermediate, and slow) observed in TACAN-transfected P1KO cells. Parentheses indicate the absolute number of occurrence of the current types. The time boundaries used for separating RA, IA, and SA currents were <5 ms, 5 < x < 50 ms, >50 ms, with a total of 55 currents.

See also Figure S3.

for TACAN. A previous study reported expression of this protein on the nuclear membrane of adipocytes (Batrakou et al., 2015). We verified the plasma membrane localization of hemagglutinin (HA)-tagged TACAN in Chinese hamster ovary (CHO) cells and sensory neuron-derived F11 cells. Our immunofluorescence and membrane biotinylation data indicate that TACAN is present at the plasma membrane (Figures S2A–S2D).

TACAN Expression Increases Mechanically Evoked Currents in Heterologous Systems

One criterion for a channel's involvement in mechanosensation is that its expression in heterologous systems should increase mechanically evoked currents (Christensen and Corey, 2007; Vollrath et al., 2007). In CHO cells stably transfected with TACAN, we used cell-attached recordings to determine whether it increases mechanically evoked currents (Figure 3A). To activate MSCs in the membrane patch under study, we applied brief pulses of negative pressure through the recording electrode. In mock-transfected CHO cells, we observed the presence of endogenous MSCs (Figure 3A, left panel). Stable expression of TACAN in CHO cells significantly increased mechanically evoked currents compared with mock-transfected cells (Figures 3A, right panel, and 3B). Although the activation threshold of the channels did not change (−33.9 ± 2.7 mm Hg, n = 31, versus −35.1 ± 3.1 mm Hg, n = 55, in mock- and TACAN-expressing cells, respectively), the percentage of active patches was significantly higher (53% versus 91% in mock- versus TACAN-expressing cells, p < 0.001, Fisher's exact test), suggesting a higher density of MSCs in TACAN-expressing cells.

In TACAN-expressing CHO cells, we determined the single-channel conductance of the MSC. Our results demonstrate that MSCs in TACAN-expressing CHO cells have a linear current-voltage (I-V) relationship with a reversal potential of 6.14 ± 2.40 mV (Figures S3A and S3B; n = 11). This is consistent with this MSC mediating a non-selective cationic conductance. These I-V relationships resulted in slope-conductance values of 11.5 ± 0.5 pS for TACAN-expressing cells (n = 11). Single-channel recordings with $CaCl_2$ as the only charge carrier demonstrated that this channel is permeable to calcium ions (Figure S3C). We further demonstrated through whole-cell

recordings that, in the absence of mechanical stimuli, TACAN expression did not affect the voltage-gated conductances in CHO cells (Figure S3D).

Endogenous MSCs are tonically inhibited through their interaction with the F-actin cytoskeleton, and destabilizing agents such as cytochalasin (Cyto-D) can increase mechanically evoked currents (Sharif-Naeini et al., 2009). We examined whether the enhanced mechanical responses observed in TACAN-expressing cells were due to TACAN removing the cytoskeletal inhibition of the endogenous MSC rather than TACAN being essential for the function of a mechanosensitive channel complex. If this was the case, then we would expect Cyto-D to significantly increase mechanically evoked currents in control cells but have little effect in TACAN-expressing cells. In control CHO cells, treatment with Cyto-D (1 μM) significantly increased mechanically evoked currents (compared with vehicle) to a level similar to that of vehicle-treated cells of the TACAN-expressing cell line (Figure S3E, left panel). However, Cyto-D treatment of TACAN-expressing cells also led to a significant increase in mechanically evoked currents, indicating that cytoskeletal inhibition of MSCs is still present in these cells and is not responsible for their increased mechanosensitivity (Figure S3E, right panel).

To determine whether this increase in cellular mechanosensitivity occurs in other cell types, we examined the effect of TACAN expression on mechanically evoked currents in HEK293 cells and COS-7 cells (Figures 3C and S3F), which are commonly used to study MSCs (Anderson et al., 2018; Coste et al., 2010; Li Fraine et al., 2017). In HEK293 cells, endogenous MSCs were present in most patches (84%, 66 of 79) and activated at a threshold of −42.0 ± 2.6 mm Hg (n = 66) to reach a plateau of activation (Figure 3C). However, when these cells were transfected with TACAN, an additional increase in mechanically activated current became evident at thresholds negative to −80 mm Hg (Figure 3C), suggesting recruitment of another MSC. This increase in mechanically evoked current did not affect the activation threshold of the first MSC (−37.1 + 3.2 mm Hg, n = 47) or the percentage of active patches (82%, 47 of 57 patches). Interestingly, the activation threshold of the second mechanically evoked current is similar to that observed for MSCs in cultured primary nociceptors (Cho et al., 2002), also known as high-threshold mechano-nociceptors. Furthermore, to eliminate any contribution from a previously documented MSC present in HEK293T cells, Piezo1, we used the recently described Piezo1 knockout cell line (Dubin et al., 2017; HEK293T-P1KO, termed P1KO cells for simplicity). Again, expression of TACAN in P1KO cells led to a significant increase in mechanically evoked currents (Figure 3D), confirming that they are independent of Piezo channels.

Interestingly, whole-cell indentation experiments did not show any TACAN-dependent, mechanically evoked current (data not shown). This is likely due to the high threshold required for TACAN activation, which is difficult to reach in flat cell lines in a culture dish without perforating the cell membrane. Such technical limitations have been reported for other MSCs (Murthy et al., 2018a; Sianati et al., 2019), and alternative means of channel activation have been developed (Poole et al., 2014; Sianati et al., 2019). We used these novel approaches to test whether TACAN can be activated by mechanical inputs applied directly at the cell-substrate interface using a pillar array analysis (Poole et al., 2014; Sianati et al., 2019). P1KO cells were transiently transfected with a plasmid encoding TACAN, and multiple mechanical inputs were applied by serially deflecting a pilus subjacent to the cell. Remarkably, large (400 pA on average) mechanically evoked currents were measured in 8 of 8 cells expressing TACAN but were absent in 9 of 9 mock-transfected controls (Figures 3E and 3F). The kinetics of these currents (latency = 1.4 ± 0.1 ms; activation time constant = 0.7 ± 0.1 ms, mean ± SEM, n = 55 currents; Figures S3G and S3H) are similar to those measured previously in nociceptors (Poole et al., 2014; Wetzel et al., 2017) and suggestive of a current directly activated by the mechanical stimulus. Previous analysis of mechanically evoked currents in nociceptors using pillar arrays demonstrated that rapid-adapting (RA), intermediate-adapting (IA), and slow-adapting (SA) currents could be evoked in a single cell and that mechanoreceptors had a low activation threshold (with deflections of less than 50 nm), whereas nociceptors required deflections between 200–1,000 nm (Poole et al., 2014). Similarly, when expressed in P1KO cells, TACAN-dependent currents exhibited variable inactivation kinetics, with the majority classified as SA (Figure 3G), and the activation threshold of the currents was in the range typically observed in nociceptors (Figures 3E and 3F).

TACAN Forms an Ion-Conducting Channel when Reconstituted in Artificial Bilayers

Our results indicate that TACAN expression increases cellular mechanosensitivity, but it remains unclear whether TACAN is an ion channel or a membrane protein that potentiates other ion channels. To determine whether expression of TACAN proteins alone is sufficient to generate an ion-conducting pore, we reconstituted isolated TACAN into lipid bilayers formed from synthetic lipids. After purification (see Table S2 for mass spectrometry analysis) and reconstitution in planar lipid bilayers, we measured the current across the membrane when voltage steps were imposed (Figure 4A). Addition of TACAN-containing proteoliposomes to the planar bilayer produced macroscopic currents (Figures 4A and S4), indicating that TACAN by itself can form an ion-conducting pore. Furthermore, the TACAN protein-elicited currents displayed Ohmic behavior (Figures 4B and 4C), similar to that observed in CHO cells expressing TACAN (Figures S3A and S3B). Finally, the TACAN channel was blocked by known blockers of MSCs, such as gadolinium (30 μM), which reduced the current to 21% and 36% of baseline at +80 mV and −80 mV, respectively (Figures 4D and 4E). The peptide GsMTx4 (5 μM), a MSC blocker purified from the venom of a Chilean rose tarantula, *Grammostola spatulata* (Bae et al., 2011; Suchyna et al., 2000), reduced the current to less than 1% of baseline. These blocker concentrations are similar to those known to inhibit endogenous MSCs (Cho et al., 2006; Drew et al., 2002; Sharif-Naeini et al., 2009; Yang and Sachs, 1989). Our results indicate that TACAN forms an ion-conducting pore that is sensitive to known blockers of MSCs.

TACAN Contributes to the Intrinsic Mechanosensitivity of Nociceptors

We next asked whether TACAN underlies the mechanosensitivity of nociceptors. Sensory DRG neurons were cultured from

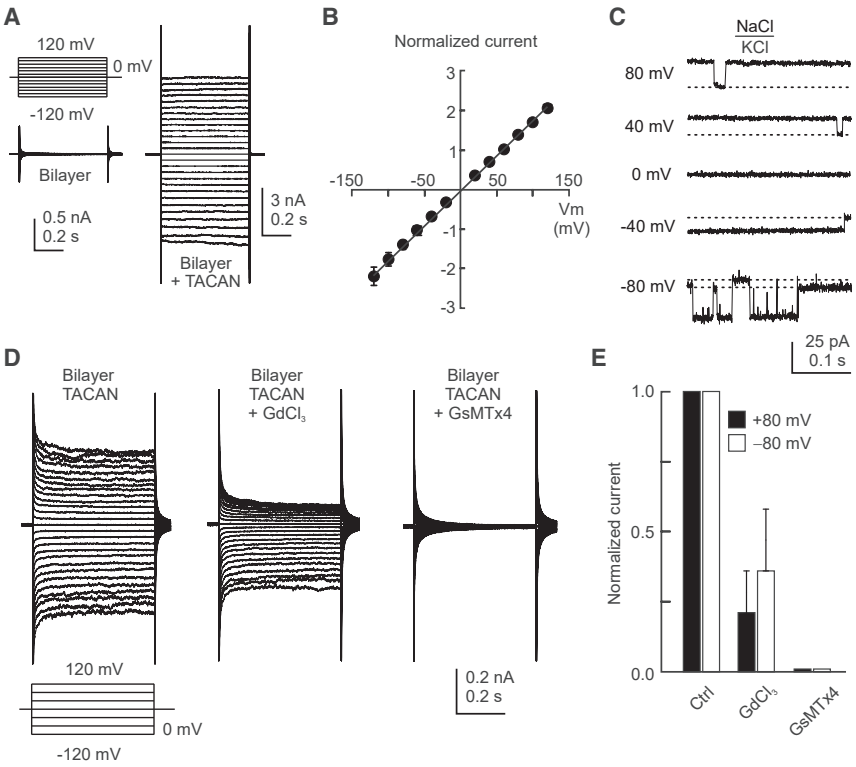

Figure 4. TACAN Forms a Functional Ion Channel in Lipid Bilayers

(A) A planar lipid bilayer showing no conductance prior to incorporation (left panel) develops macroscopic currents (right panel) after insertion of purified and reconstituted TACAN channels. Traces show currents in response to voltage pulses from a resting value of 0 mV to voltages between −120 and +120 mV at intervals of 10 mV.

(B) Mean (± SD, n = 7) current normalized to the current value at +80 mV. The I-V relation is consistent with a non-selective cation channel.

(C) Single-channel recordings of reconstituted TACAN under divalent-free conditions.

(D) The conductance is sensitive to gadolinium ($GdCl_3$; 30 μM) and GsMTx4 (5 μM).

(E) Bilayer current (normalized to pre-blocker current) after addition of $GdCl_3$ or GsMTx4.

See also Figure S4 and Table S2.

reporter mice in which nociceptors were visually identifiable through expression of tdTomato. Neurons were transfected with Alexa 488-labeled small interfering RNA (siRNA) molecules targeting TACAN or a non-targeting (NT) control (Figure 5A). The knockdown was validated using a neuroblastoma (N2A) cell line (Coste et al., 2010; Figures S5A and S5B). Our data demonstrated that reducing the expression level of TACAN leads to a significant reduction in mechanically evoked currents in nociceptors (Figures 5B–5D). This decrease was accompanied by a significant reduction in the number of patches with active MSCs (44 of 54 [81%] in NT siRNA compared with 40 of 67 (59%) in TACAN siRNA-transfected nociceptors, Fisher's exact probability test, $p = 0.008$). To determine whether mechanically evoked currents in nociceptors share the same pharmacological sensitivity as purified TACAN in synthetic lipids, we examined the nociceptors' sensitivity to GsMTx4. Our data demonstrated that, in outside-out recordings from nociceptors, superfusion of GsMTx4 led to a significant and reversible block of mechanically evoked currents (Figures 5E and 5F). Importantly, the concentration used in this experiment was the same as the one used to block TACAN-elicited currents in the bilayer (5 μM).

Mechanically evoked whole-cell currents in nociceptors display unique non-adapting or ultra-slow adapting kinetics that distinguish them from the rapidly adapting currents recorded mainly in large-diameter, touch-sensitive mechanoreceptors (Hao and Delmas, 2010). The latter has been associated with expression of Piezo2 (Ranade et al., 2014b; Woo et al., 2015). To determine whether TACAN contributes to the ultra-slow adapting current in nociceptors, we recorded whole-cell mechanically evoked currents from DRG neurons obtained from wild-type mice, transfected with the same set of Alexa 488-labeled siRNA molecules. We defined three types of whole-cell currents based on their inactivation kinetics (Figure 5G; Francois et al., 2015). Compared with NT siRNA-transfected neurons (n = 21), treatment of DRG neurons with TACAN siRNA (n = 31) caused a significant ($p < 0.05$, Fisher's exact probability test) decrease in the proportion of neurons displaying the ultra-slow adapting current (Figure 5H). We observed an increase, although non-significant, in the proportion of neurons displaying no or mixed currents in the TACAN siRNA-treated group, as predicted if the loss of TACAN converts ultra-slow adapting neurons into mixed or non-responders.

TACAN Is Involved in Detection of Painful Mechanical Stimuli *In Vivo*

We next asked whether TACAN is necessary for detection of painful mechanical stimuli. We hypothesized that reducing TACAN expression would impair responses to high-intensity mechanical stimuli but not to low-intensity stimuli. Furthermore, the response to non-mechanical nociceptive stimuli, such as heat, should be unaffected. The difficulties in addressing this question are that (1) global knockout of TACAN is embryonically lethal and (2) the need for mechanotransduction during tissue morphogenesis (Farge, 2011) is such that even tissue-specific embryonic deletion may affect neuronal pathfinding (Jacques-Fricke et al., 2006). We therefore generated a conditional, tamoxifen-inducible TACAN knockout mouse by crossing $Mrgprd^{CreERT2}$ mice to TACAN floxed ($TACAN^{fl/fl}$) mice (termed $TACAN^{cKO}$ for simplicity). The Cre driver line was chosen because of the high co-labeling of TACAN-positive DRG neurons with the non-peptidergic population. Administration of tamoxifen caused a significant reduction in TACAN expression in this nociceptor population (Figures S2E–S2H).

In mice, the typical behavioral responses to hindpaw stimulation with mechanical stimuli of increasing intensity can be

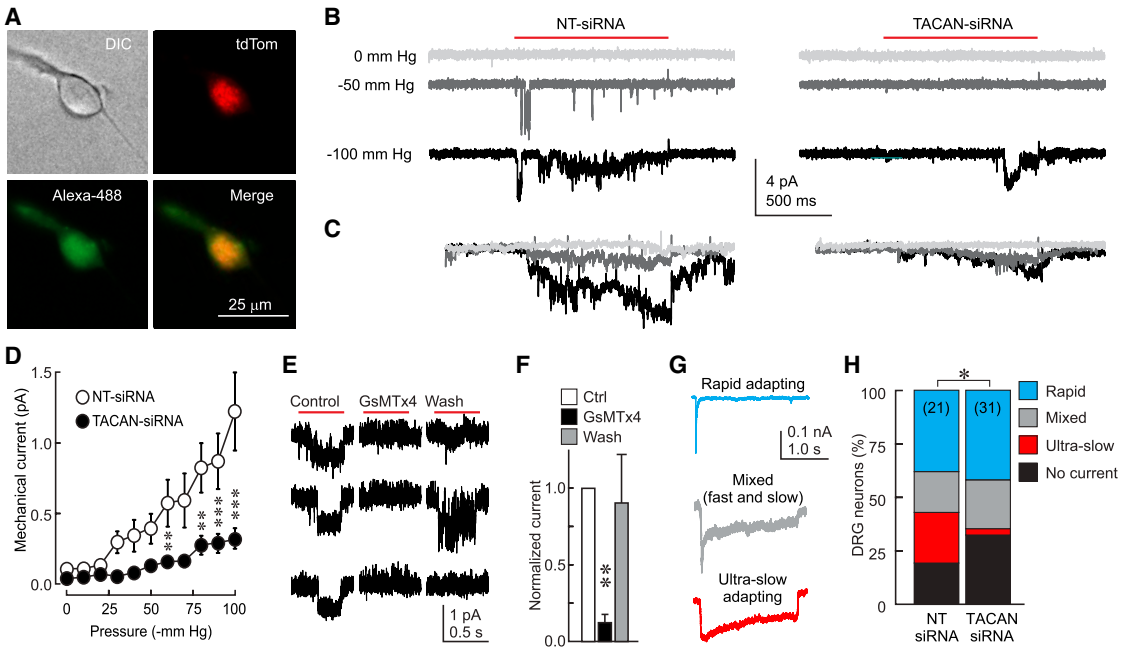

Figure 5. TACAN Contributes to the Mechanosensitivity of Nociceptors

(A) Representative image of a cultured nociceptor from a *Trpv1-tdTom* mouse transfected with Alexa 488-conjugated siRNA molecules targeting TACAN.

(B) Representative mechanically evoked, cell-attached currents in cultured nociceptors 72 h after transfection of control (NT siRNA) or TACAN-targeting siRNA molecules.

(C) Average current traces of mechanically evoked responses in nociceptors transfected with NT or TACAN siRNA (n = 77 and 66 cells, respectively).

(D) Mean (± SEM) mechanically evoked currents in nociceptors transfected with NT or TACAN-targeting siRNA. **p < 0.01, ***p < 0.001, respectively. Asterisks indicate significant difference from the NT siRNA group (two-way ANOVA with Tukey post hoc test).

(E) Representative mechanically evoked currents obtained from DRG neurons in the outside-out configuration in response to a positive pressure pulse from the recording pipette (red bar) before (control), during (GsMTx4), and after (wash) application of 5 μM GsMTx4. The three rows represent repetitive trials under each condition.

(F) Mean (± SEM) mechanically evoked currents extracted from the approach depicted in (E) (n = 6).

(G) Representative types of mechanically evoked whole-cell currents from cultured DRG neurons stimulated by an indenting stimulus from a blunt probe.

(H) Percentages of neurons displaying the response types shown in (G) (n = 21 and 31 neurons under NT and TACAN siRNA conditions, respectively; *p < 0.05, contingency test with Fisher's exact probability test).

See also Figure S5.

divided as follows: (1) no response; (2) detection, during which there is slight stretching of the digits without withdrawal; (3) reflex-type withdrawal; and (4) a nocifensive response consisting of withdrawal followed by licking of the hindpaw. Control mice included TACAN$^{fl/fl}$ with tamoxifen and Mrgprd^{CreERT2} TACAN$^{fl/fl}$ without tamoxifen. In the latter, mechanical stimulation of the hindpaw with increasing intensity led to an increase in the frequency of withdrawal reflexes until the intensity exceeded 1.00–1.40 g, after which these behavioral responses decreased and were replaced by nocifensive responses (Figure 6A). Interestingly, following tamoxifen injection (TACAN^{cKO}), the mice continued to display reflex-type withdrawals despite increasing stimulus intensity (Figure 6A). This was confirmed by a significant decrease in the nocifensive behaviors observed in the TACAN^{cKO} mice following tamoxifen injection (Figure 6B). When examining the proportion of responses to a 1-g stimulus in TACAN$^{fl/fl}$ and TACAN^{cKO} mice before and after administration of tamoxifen, we observed a significant decrease in nocifensive responses (Figure 6C). This indicates that the expression of TACAN in non-peptidergic nociceptors contributes to the sensation of mechanical pain. In its absence, high-intensity mechanical stimuli would only produce reflex-type responses.

Because the expression of TACAN at the mRNA level indicates a distribution that extends to other subsets of DRG neurons, including mechanoreceptors (Zeisel et al., 2018), we examined whether reducing its expression in a broader population would also generate defects in touch sensing. We injected AAV2/6 viral particles expressing a short hairpin RNA (shRNA) targeting TACAN or a NT control directly into the left sciatic nerve bundle of wild-type (WT) mice. We hypothesized that knocking down TACAN expression in mechanoreceptors would affect the withdrawal reflex as well. Knockdown of TACAN by the virus was validated in F11 cells (Figures S5C and S5D). However, again, despite the fact that broader knockdown was produced, the reduction in TACAN expression specifically affected nocifensive responses and had no effect on reflex withdrawals (Figure 6D). Finally, to account for a partial knockdown effect of the shRNA virus, we repeated the procedure and injected AAV particles carrying the Cre recombinase under the synapsin promoter in the sciatic nerve bundle of TACAN$^{fl/fl}$ mice. Again, the behavioral

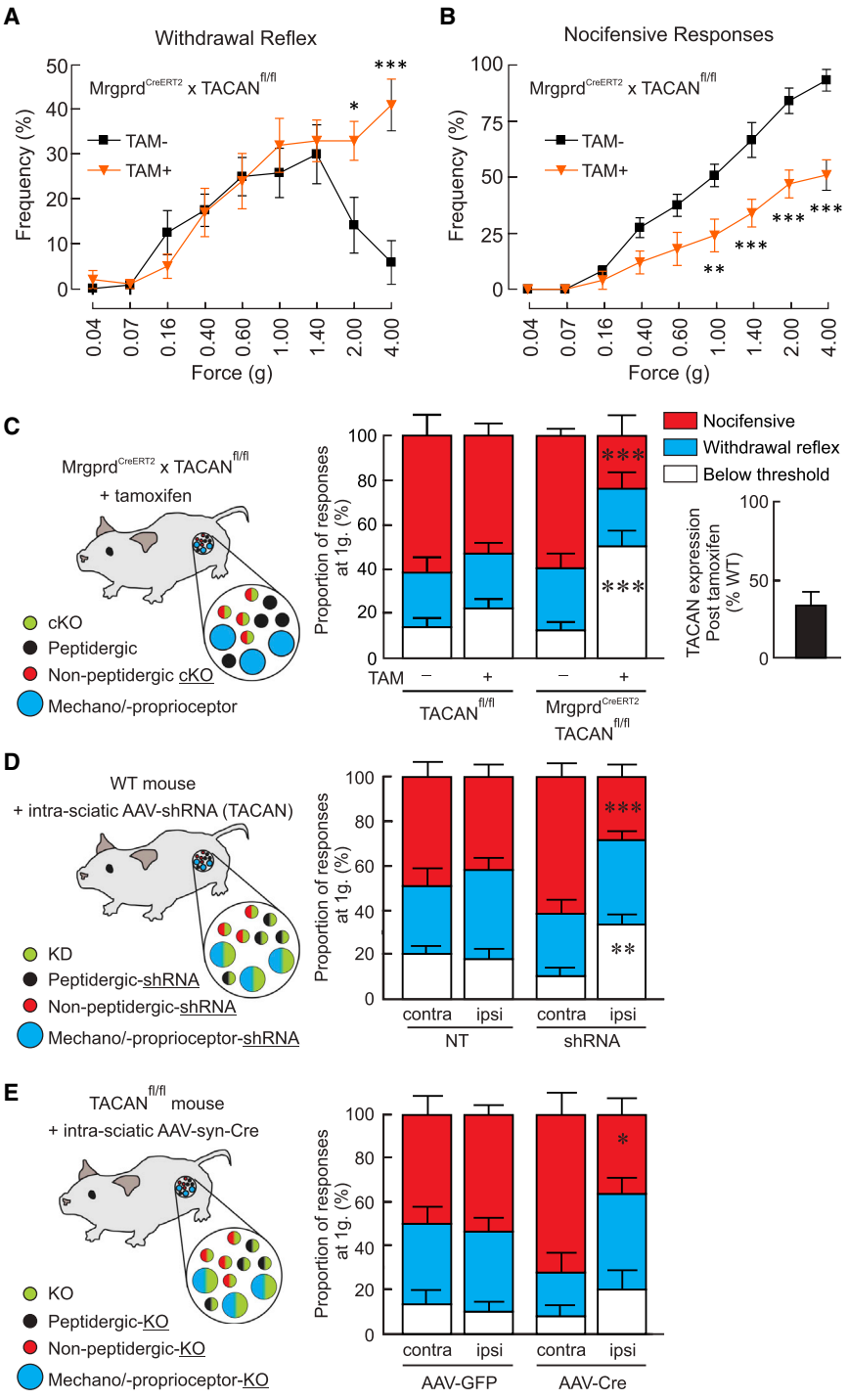

Figure 6. TACAN Deletion Impairs the Detection of Painful Mechanical Stimuli *In Vivo*

(A) Mean (± SEM) frequency of mechanically elicited reflexive paw withdrawal in response to application of von Frey filaments of increasing intensity in Mrgprd^{CreERT2} × TACAN$^{fl/fl}$ before (black trace, n = 6), and 5 weeks after (orange trace, n = 5) tamoxifen injection.

(B) Mean (± SEM) frequency of mechanically elicited nocifensive behaviors in response to application of von Frey filaments of increasing intensity in Mrgprd^{CreERT2} × TACAN$^{fl/fl}$ before (black trace, n = 6), and 5 weeks after (orange trace, n = 5) tamoxifen injection.

For both (A) and (B) *p < 0.05, **p < 0.01, ***p < 0.001. Asterisks indicate significant difference from the WT group (two-way ANOVA with Bonferroni post hoc test).

(C–E) Left: representative cartoons of the site of TACAN deletion (green). (C) Distribution of behavioral responses to a 1-g stimulation of the hindpaw in TACAN$^{fl/fl}$ (n = 6) or Mrgprd^{CreERT2} × TACAN$^{fl/fl}$ (n = 5) mice before or 5 weeks after systemic administration of tamoxifen. Mrgprd^{CreERT2} × TACAN$^{fl/fl}$ mice display selective loss of nocifensive responses that is replaced by an increase in the proportion of responses below the withdrawal threshold (no response and detection responses combined; STAR Methods). Inset: the decrease in TACAN mRNA in DRGs after tamoxifen injection, expressed as percentage of tamoxifen-injected WT mice (n = 3). (D) Unilateral and non-specific knockdown of TACAN in all sensory neurons of WT mice (C57BL/6) with AAVs carrying TACAN-targeting shRNA (n = 13) molecules or NT controls (n = 12). Shown is the distribution of behavioral responses to a 1-g stimulus. Measurements were done 4 weeks post-virus injection. **p < 0.01, ***p < 0.001. (E) Distribution of behavioral responses to 1-g stimulation of the hindpaw in TACAN$^{fl/fl}$ mice injected unilaterally with AAVs carrying the Cre recombinase (AAV-Cre, n = 5) or GFP (AAV-GFP, n = 6). Measurements were done 4 weeks post-virus injection. For (C–E), *p < 0.05, **p < 0.01, ***p < 0.001. Asterisks indicate significant difference between ipsilateral and contralateral paws (Fischer's exact test).

See also Figure S5.

phenotype was specific loss of nocifensive responses to mechanical stimuli (Figure 6E).

Interestingly, the loss of nocifensive responses in the absence of TACAN was specific to mechanical stimuli because the same mice continued to exhibit normal nociceptive responses to painful thermal stimuli (Hargreaves' test; Figures S5F and S5I). Finally, reflexive paw withdrawal from a pinprick stimulus, a model of intense mechanical pain stimuli depending on peptidergic A-δ nociceptors (Arcourt et al., 2017), was not different in the two groups (Figures S5G and S5J), suggesting that A-δ nociceptors may express a MSC other than TACAN. Taken together, these data indicate that TACAN is involved in detection of painful mechanical stimuli.

DISCUSSION

Despite recent advances in understanding the ionic mechanisms responsible for our sense of hearing (Pan et al., 2018), touch

(Ranade et al., 2014b), and proprioception (Woo et al., 2015), the mechanisms responsible for our sense of mechanical pain have remained elusive. In this study, we identified an ion channel that is specifically involved in sensing painful mechanical stimuli without affecting sensitivity to touch or heat stimuli.

For a candidate channel to be considered intrinsically mechanosensitive, it should (1) be expressed in mechanosensitive cells; (2) be expressed at the plasma membrane; (3) increase mechanosensitivity when expressed in heterologous systems; (4) require gating stimuli similar to those in native cells (nociceptors); (5) display rapid opening (<5 ms); (6) cause a decrease in mechanosensitivity when its expression is reduced in native cells; (7) form an ion-conducting pore when reconstituted in synthetic membranes and remain gated by mechanical stimuli; and (8) its deletion *in vivo* should cause mechanosensing defects (Christensen and Corey, 2007; Vollrath et al., 2007).

Our results indicate that TACAN satisfies at least 7 of these 8 conditions. It increases cell-attached and whole-cell mechanically induced currents in heterologous systems, and its downregulation impairs the mechanosensitivity of nociceptors. The purified TACAN protein reconstituted in synthetic lipids forms a functional channel that is blocked by known MSC blockers. Finally, reducing or knocking out TACAN expression in sensory neurons selectively impairs the ability of mice to sense painful mechanical stimuli without affecting their sensitivity to touch or heat. Loss of nocifensive responses to mechanical stimuli when TACAN is removed in the adult is similar to ablation of Mrgprd-positive non-peptidergic nociceptive fibers in the adult mouse, where the frequency of withdrawals to an ascending set of von Frey filaments becomes significantly different when the filament intensity exceeds 1.0 g (Cavanaugh et al., 2009).

Interestingly, in single-channel recordings, the conductance values for TACAN were higher in bilayers than in cell lines. This could be due to the fact that, in the bilayer system, the channel is purified and does not have any interacting partners that could affect its conductance. Although the high conductance observed in single-channel openings in the bilayer recordings may be reminiscent of porins, their presence in the bilayer preparation is unlikely because (1) they were not detected in the mass spectrometry analysis; (2) porin conductance (0.8–4.0 nS) (Kreir et al., 2008; Mahendran et al., 2010; Trias and Benz, 1993) is much higher than the one observed here; and (3) porins tend to close at high membrane voltages, whereas this channel remains linear. Furthermore, our macroscopic currents were sensitive to GsMTx4 and GdCl3.

Naturally, we were not able to apply mechanical stimuli to the purified TACAN in the planar lipid bilayer and therefore cannot comment on its intrinsic mechanosensitivity. Nonetheless, given that membrane tension is proportional to the radius of curvature (Sachs and Morris, 1998), one would expect the planar bilayer to exert enough tension to maintain the channel in the open configuration (Figure S4). Future experiments in reconstituted proteoliposomes are needed to test whether TACAN has intrinsic mechanosensitive properties or needs other proteins.

It was recently proposed that the MSC Piezo2 mediates sensitivity to mechanical pain in mice (Murthy et al., 2018b) because its deletion in all caudal sensory neurons ($HoxB8^{Cre}$;;$Piezo2^{fl/fl}$ mice) impaired nocifensive responses to painful mechanical stimuli. However, several lines of evidence complicate interpretation of those findings: (1) the gait phenotype of mice is significantly impaired (Video S4 in Woo et al., 2015), (2) the slow-adapting currents are not affected in nociceptors, and (3) embryonic deletion of Piezo2 may disrupt proper development of the nervous system. Furthermore, two recent studies support a role for Piezo2 in transducing touch but not pain (Szczot et al., 2018; Zhang et al., 2019).

TACAN defines a previously uncharacterized class of ion channels. Much like the Piezo family of MSC, which was found to be involved in touch (Ranade et al., 2014b), proprioception (Woo et al., 2015), lung inflation (Nonomura et al., 2017), vascular development (Ranade et al., 2014a), and red blood cell volume regulation (Cahalan et al., 2015; Ma et al., 2018), TACAN is expressed in many tissues and is likely to play important roles in several mechanotransduction processes. TACAN also has a homolog in mammalian cells, TMEM120B, but its heterologous expression did not increase mechanically evoked currents (Figures S3I–S3K). Our bilayer reconstitution experiments indicate that TACAN can form an ion channel by itself but that TMEM120B may act as an accessory subunit to TACAN.

Activation of nociceptors is central to the experience of pain, and several chronic pain conditions are caused by the sensitization of nociceptors to mechanical stimuli, including osteoarthritis and rheumatoid arthritis pain (He et al., 2017; McQueen et al., 1991; Neogi et al., 2016; Okun et al., 2012; Schaible, 2014). Intervening at the level of primary afferent nociceptors is a promising approach to developing therapeutic treatments. However, pain management in many of these chronic inflammatory conditions is currently inadequate, in part because the identity of the ion channels involved in pain transduction has remained elusive. With the discovery of TACAN, we identified a potential therapeutic target in the treatment of chronic inflammatory pain.

STAR★METHODS

Detailed methods are provided in the online version of this paper and include the following:

- KEY RESOURCES TABLE
- LEAD CONTACT AND MATERIALS AVAILABILITY
- EXPERIMENTAL MODEL AND SUBJECT DETAILS
  - C57BL/6 Mice
  - Trpv1-tdTom mice
  - Human dorsal root ganglia
  - COS7 cells
  - Piezo1 KO cells
  - Stable CHO cell generation
  - Mouse DRG culture
- METHOD DETAILS
  - *In Situ* Hybridization
  - Generation of an affinity-purified rabbit antibody against TACAN
  - Immunohistochemistry
  - Cell-attached recordings
  - Whole-cell recordings with mechanical stimulation via cell indentations

- Whole-cell recordings with mechanical stimulation via micropillar substrate deflection
- Outside-out recordings and GsMTx4 treatment
- Bilayer recordings
- TACAN purification
- Mass Spectrometry of purified TACAN
- CHO HA-TACAN membrane staining and imaging
- Biotinylation on CHO stable cell line
- Knockdown of TACAN *in vitro* and *in vivo*
- Von Frey filament test
- Hargreaves plantar test
- Pinprick test

- QUANTIFICATION AND STATISTICAL ANALYSIS
- DATA AND CODE AVAILABILITY

SUPPLEMENTAL INFORMATION

Supplemental Information can be found online at https://doi.org/10.1016/j.cell.2020.01.033.

ACKNOWLEDGMENTS

This work was supported by operating grants from the Canadian Institutes of Health Research, a pilot grant from the Groupe d'Etude des Protéines Membranaires (GEPROM), and a salary award from the Fonds de Recherche du Quebec-Santé (to R.S.-N.). E.B. was supported by grants from the Fondation pour la Recherche Médicale (Équipe FRM 2015) and the Agence Nationale pour la Recherche (ANR15-CE16-0012-01 and LABEX ICST). A.R.-d.-S. was supported by an operating grant from the Canadian Institutes of Health Research (MOP-136903). K.P. was partially supported by NHMRC project grant APP1122104. M.C. and N.Y. were supported by fellowships from the Louise and Alan Edwards Foundation. L.B.-L. is supported by the Natural Sciences and Engineering Research Council of Canada (NSERC) (PGSD2-517068-2018). K.A. was supported by the Ontario Thoracic Society and the Canada Foundation for Innovation John R. Evans Leaders Fund (31979).

AUTHOR CONTRIBUTIONS

L.B.-L. performed and analyzed electrophysiological recordings in heterologous cell lines and nociceptors. He also contributed to manuscript and figure preparation. M.C. performed and analyzed electrophysiological recordings in heterologous cell lines and behavior experiments. A. Donoghue performed bilayer experiments. F.A. and E.B. performed whole-cell DRG recordings. N.Y., T.F., and A.R.-d.-S. performed immunohistochemistry experiments. H.P. performed *in situ* hybridization and behavior experiments. A. Davidova performed *in situ* experiments, immunostaining, cell culture, and transfection; validated siRNA and shRNA; and generated stable cell lines. C.S. performed COS-7 recordings. U.K. and C.D. performed HEK293 recordings. E.F. performed TACAN purification experiments for bilayer recordings. A.M. performed TACAN membrane localization experiments. S.M.-C., D.G.B., L.H., J.A.O., and L.S.S. dissected human DRG from donors. J.S. provided *in situ* probes for human TACAN. M.-J.S. and K.A. performed ISH on human DRGs. R.B. supervised bilayer experiments. K.P. performed whole-cell TACAN experiments on pillars. R.S.-N. designed experiments, supervised the project, and prepared the manuscript.

DECLARATION OF INTERESTS

R.S.-N. has a patent (US9551718B2) related to this work.

Received: July 22, 2019
Revised: November 8, 2019
Accepted: January 29, 2020
Published: February 20, 2020

REFERENCES

Anderson, E.O., Schneider, E.R., Matson, J.D., Gracheva, E.O., and Bagriantsev, S.N. (2018). TMEM150C/Tentonin3 Is a Regulator of Mechano-gated Ion Channels. Cell Rep. *23*, 701–708.

Arcourt, A., Gorham, L., Dhandapani, R., Prato, V., Taberner, F.J., Wende, H., Gangadharan, V., Birchmeier, C., Heppenstall, P.A., and Lechner, S.G. (2017). Touch Receptor-Derived Sensory Information Alleviates Acute Pain Signaling and Fine-Tunes Nociceptive Reflex Coordination. Neuron *93*, 179–193.

Bae, C., Sachs, F., and Gottlieb, P.A. (2011). The mechanosensitive ion channel Piezo1 is inhibited by the peptide GsMTx4. Biochemistry *50*, 6295–6300.

Batrakou, D.G., de Las Heras, J.I., Czapiewski, R., Mouras, R., and Schirmer, E.C. (2015). TMEM120A and B: Nuclear Envelope Transmembrane Proteins Important for Adipocyte Differentiation. PLoS ONE *10*, e0127712.

Bourque, C.W. (2008). Central mechanisms of osmosensation and systemic osmoregulation. Nat. Rev. Neurosci. *9*, 519–531.

Boyer, A.E., Quinn, C.P., Beesley, C.A., Gallegos-Candela, M., Marston, C.K., Cronin, L.X., Lins, R.C., Stoddard, R.A., Li, H., Schiffer, J., et al. (2011). Lethal factor toxemia and anti-protective antigen antibody activity in naturally acquired cutaneous anthrax. J. Infect. Dis. *204*, 1321–1327.

Cahalan, S.M., Lukacs, V., Ranade, S.S., Chien, S., Bandell, M., and Patapoutian, A. (2015). Piezo1 links mechanical forces to red blood cell volume. eLife *4*, e07370.

Cavanaugh, D.J., Lee, H., Lo, L., Shields, S.D., Zylka, M.J., Basbaum, A.I., and Anderson, D.J. (2009). Distinct subsets of unmyelinated primary sensory fibers mediate behavioral responses to noxious thermal and mechanical stimuli. Proc. Natl. Acad. Sci. USA *106*, 9075–9080.

Chalfie, M. (2009). Neurosensory mechanotransduction. Nat. Rev. Mol. Cell Biol. *10*, 44–52.

Chen, Y., Simasko, S.M., Niggel, J., Sigurdson, W.J., and Sachs, F. (1996). Ca2+ uptake in GH3 cells during hypotonic swelling: the sensory role of stretch-activated ion channels. Am. J. Physiol. *270*, C1790–C1798.

Cho, H., Shin, J., Shin, C.Y., Lee, S.Y., and Oh, U. (2002). Mechanosensitive ion channels in cultured sensory neurons of neonatal rats. J. Neurosci. *22*, 1238–1247.

Cho, H., Koo, J.Y., Kim, S., Park, S.P., Yang, Y., and Oh, U. (2006). A novel mechanosensitive channel identified in sensory neurons. Eur. J. Neurosci. *23*, 2543–2550.

Christensen, A.P., and Corey, D.P. (2007). TRP channels in mechanosensation: direct or indirect activation? Nat. Rev. Neurosci. *8*, 510–521.

Coste, B., Mathur, J., Schmidt, M., Earley, T.J., Ranade, S., Petrus, M.J., Dubin, A.E., and Patapoutian, A. (2010). Piezo1 and Piezo2 are essential components of distinct mechanically activated cation channels. Science *330*, 55–60.

Delfini, M.C., Mantilleri, A., Gaillard, S., Hao, J., Reynders, A., Malapert, P., Alonso, S., François, A., Barrere, C., Seal, R., et al. (2013). TAFA4, a chemokine-like protein, modulates injury-induced mechanical and chemical pain hypersensitivity in mice. Cell Rep. *5*, 378–388.

Drew, L.J., Wood, J.N., and Cesare, P. (2002). Distinct mechanosensitive properties of capsaicin-sensitive and -insensitive sensory neurons. J. Neurosci. *22*, RC228.

Dubin, A.E., Murthy, S., Lewis, A.H., Brosse, L., Cahalan, S.M., Grandl, J., Coste, B., and Patapoutian, A. (2017). Endogenous Piezo1 Can Confound Mechanically Activated Channel Identification and Characterization. Neuron *94*, 266–270.e3.

Ducourneau, V.R., Dolique, T., Hachem-Delaunay, S., Miraucourt, L.S., Amadio, A., Blaszczyk, L., Jacquot, F., Ly, J., Devoize, L., Oliet, S.H., et al. (2014). Cancer pain is not necessarily correlated with spinal overexpression of reactive glia markers. Pain *155*, 275–291.

Farge, E. (2011). Mechanotransduction in development. Curr. Top. Dev. Biol. *95*, 243–265.

Faure, É., Starek, G., McGuire, H., Bernèche, S., and Blunck, R. (2012). A limited 4 Å radial displacement of the S4-S5 linker is sufficient for internal gate closing in Kv channels. J. Biol. Chem. *287*, 40091–40098.

Francois, A., Schuetter, N., Laffray, S., Sanguesa, J., Pizzoccaro, A., Dubel, S., Mantilleri, A., Nargeot, J., Noel, J., Wood, J.N., et al. (2015). The Low-Threshold Calcium Channel Cav3.2 Determines Low-Threshold Mechanoreceptor Function. Cell Rep. *10*, 370–382.

Gaillard, S., Lo Re, L., Mantilleri, A., Hepp, R., Urien, L., Malapert, P., Alonso, S., Deage, M., Kambrun, C., Landry, M., et al. (2014). GINIP, a Gαi-interacting protein, functions as a key modulator of peripheral GABAB receptor-mediated analgesia. Neuron *84*, 123–136.

Hao, J., and Delmas, P. (2010). Multiple desensitization mechanisms of mechanotransducer channels shape firing of mechanosensory neurons. J. Neurosci. *30*, 13384–13395.

Hargreaves, K., Dubner, R., Brown, F., Flores, C., and Joris, J. (1988). A new and sensitive method for measuring thermal nociception in cutaneous hyperalgesia. Pain *32*, 77–88.

He, B.H., Christin, M., Mouchbahani-Constance, S., Davidova, A., and Sharif-Naeini, R. (2017). Mechanosensitive ion channels in articular nociceptors drive mechanical allodynia in osteoarthritis. Osteoarthritis Cartilage *25*, 2091–2099.

Hong, G.S., Lee, B., Wee, J., Chun, H., Kim, H., Jung, J., Cha, J.Y., Riew, T.R., Kim, G.H., Kim, I.B., and Oh, U. (2016). Tentonin 3/TMEM150c Confers Distinct Mechanosensitive Currents in Dorsal-Root Ganglion Neurons with Proprioceptive Function. Neuron *91*, 107–118.

Hu, J., and Lewin, G.R. (2006). Mechanosensitive currents in the neurites of cultured mouse sensory neurones. J. Physiol. *577*, 815–828.

Jacques-Fricke, B.T., Seow, Y., Gottlieb, P.A., Sachs, F., and Gomez, T.M. (2006). Ca2+ influx through mechanosensitive channels inhibits neurite outgrowth in opposition to other influx pathways and release from intracellular stores. J. Neurosci. *26*, 5656–5664.

Keller, A., Nesvizhskii, A.I., Kolker, E., and Aebersold, R. (2002). Empirical statistical model to estimate the accuracy of peptide identifications made by MS/MS and database search. Anal. Chem. *74*, 5383–5392.

Kreir, M., Farre, C., Beckler, M., George, M., and Fertig, N. (2008). Rapid screening of membrane protein activity: electrophysiological analysis of OmpF reconstituted in proteoliposomes. Lab Chip *8*, 587–595.

Li, M.F., Hsiao, C.H., Chen, Y.L., Huang, W.Y., Lee, Y.H., Huang, H.N., and Lien, H.C. (2012). Human herpesvirus 8-associated lymphoma mimicking cutaneous anaplastic large T-cell lymphoma in a patient with human immunodeficiency virus infection. J. Cutan. Pathol. *39*, 274–278.

Li Fraine, S., Patel, A., Duprat, F., and Sharif-Naeini, R. (2017). Dynamic regulation of TREK1 gating by Polycystin 2 via a Filamin A-mediated cytoskeletal Mechanism. Sci. Rep. *7*, 17403.

Ma, S., Cahalan, S., LaMonte, G., Grubaugh, N.D., Zeng, W., Murthy, S.E., Paytas, E., Gamini, R., Lukacs, V., Whitwam, T., et al. (2018). Common PIEZO1 Allele in African Populations Causes RBC Dehydration and Attenuates Plasmodium Infection. Cell *173*, 443–455.e12.

Mahendran, K.R., Kreir, M., Weingart, H., Fertig, N., and Winterhalter, M. (2010). Permeation of antibiotics through Escherichia coli OmpF and OmpC porins: screening for influx on a single-molecule level. J. Biomol. Screen. *15*, 302–307.

McQueen, D.S., Iggo, A., Birrell, G.J., and Grubb, B.D. (1991). Effects of paracetamol and aspirin on neural activity of joint mechanonociceptors in adjuvant arthritis. Br. J. Pharmacol. *104*, 178–182.

Murthy, S.E., Dubin, A.E., Whitwam, T., Jojoa-Cruz, S., Cahalan, S.M., Mousavi, S.A.R., Ward, A.B., and Patapoutian, A. (2018a). OSCA/TMEM63 are an Evolutionarily Conserved Family of Mechanically Activated Ion Channels. eLife *7*.

Murthy, S.E., Loud, M.C., Daou, I., Marshall, K.L., Schwaller, F., Kühnemund, J., Francisco, A.G., Keenan, W.T., Dubin, A.E., Lewin, G.R., and Patapoutian, A. (2018b). The mechanosensitive ion channel Piezo2 mediates sensitivity to mechanical pain in mice. Sci. Transl. Med. *10*.

Neogi, T., Guermazi, A., Roemer, F., Nevitt, M.C., Scholz, J., Arendt-Nielsen, L., Woolf, C., Niu, J., Bradley, L.A., Quinn, E., and Law, L.F. (2016). Association of Joint Inflammation With Pain Sensitization in Knee Osteoarthritis: The Multicenter Osteoarthritis Study. Arthritis Rheumatol. *68*, 654–661.

Nesvizhskii, A.I., Keller, A., Kolker, E., and Aebersold, R. (2003). A statistical model for identifying proteins by tandem mass spectrometry. Anal. Chem. *75*, 4646–4658.

Nonomura, K., Woo, S.H., Chang, R.B., Gillich, A., Qiu, Z., Francisco, A.G., Ranade, S.S., Liberles, S.D., and Patapoutian, A. (2017). Piezo2 senses airway stretch and mediates lung inflation-induced apnoea. Nature *541*, 176–181.

Okun, A., Liu, P., Davis, P., Ren, J., Remeniuk, B., Brion, T., Ossipov, M.H., Xie, J., Dussor, G.O., King, T., and Porreca, F. (2012). Afferent drive elicits ongoing pain in a model of advanced osteoarthritis. Pain *153*, 924–933.

Pan, B., Géléoc, G.S., Asai, Y., Horwitz, G.C., Kurima, K., Ishikawa, K., Kawashima, Y., Griffith, A.J., and Holt, J.R. (2013). TMC1 and TMC2 are components of the mechanotransduction channel in hair cells of the mammalian inner ear. Neuron *79*, 504–515.

Pan, B., Akyuz, N., Liu, X.P., Asai, Y., Nist-Lund, C., Kurima, K., Derfler, B.H., Gyorgy, B., Limapichat, W., Walujkar, S., et al. (2018). TMC1 Forms the Pore of Mechanosensory Transduction Channels in Vertebrate Inner Ear Hair Cells. Neuron *99*, 736–753.e6.

Peyronnet, R., Sharif-Naeini, R., Folgering, J.H., Arhatte, M., Jodar, M., El Boustany, C., Gallian, C., Tauc, M., Duranton, C., Rubera, I., et al. (2012). Mechanoprotection by polycystins against apoptosis is mediated through the opening of stretch-activated K(2P) channels. Cell Rep. *1*, 241–250.

Poole, K., Herget, R., Lapatsina, L., Ngo, H.D., and Lewin, G.R. (2014). Tuning Piezo ion channels to detect molecular-scale movements relevant for fine touch. Nat. Commun. *5*, 3520.

Ranade, S.S., Qiu, Z., Woo, S.H., Hur, S.S., Murthy, S.E., Cahalan, S.M., Xu, J., Mathur, J., Bandell, M., Coste, B., et al. (2014a). Piezo1, a mechanically activated ion channel, is required for vascular development in mice. Proc. Natl. Acad. Sci. USA *111*, 10347–10352.

Ranade, S.S., Woo, S.H., Dubin, A.E., Moshourab, R.A., Wetzel, C., Petrus, M., Mathur, J., Bégay, V., Coste, B., Mainquist, J., et al. (2014b). Piezo2 is the major transducer of mechanical forces for touch sensation in mice. Nature *516*, 121–125.

Sachs, F., and Morris, C.E. (1998). Mechanosensitive ion channels in nonspecialized cells. Rev. Physiol. Biochem. Pharmacol. *132*, 1–77.

Schaible, H.G. (2014). Nociceptive neurons detect cytokines in arthritis. Arthritis Res. Ther. *16*, 470.

Sharif-Naeini, R., Folgering, J.H., Bichet, D., Duprat, F., Lauritzen, I., Arhatte, M., Jodar, M., Dedman, A., Chatelain, F.C., Schulte, U., et al. (2009). Polycystin-1 and -2 dosage regulates pressure sensing. Cell *139*, 587–596.

Sianati, S., Kurumlian, A., Bailey, E., and Poole, K. (2019). Analysis of Mechanically Activated Ion Channels at the Cell-Substrate Interface: Combining Pillar Arrays and Whole-Cell Patch-Clamp. Front. Bioeng. Biotechnol. *7*, 47.

Suchyna, T.M., Johnson, J.H., Hamer, K., Leykam, J.F., Gage, D.A., Clemo, H.F., Baumgarten, C.M., and Sachs, F. (2000). Identification of a peptide toxin from Grammostola spatulata spider venom that blocks cation-selective stretch-activated channels. J. Gen. Physiol. *115*, 583–598.

Szczot, M., Liljencrantz, J., Ghitani, N., Barik, A., Lam, R., Thompson, J.H., Bharucha-Goebel, D., Saade, D., Necaise, A., Donkervoort, S., et al. (2018). PIEZO2 mediates injury-induced tactile pain in mice and humans. Sci. Transl. Med. *10*.

Trias, J., and Benz, R. (1993). Characterization of the channel formed by the mycobacterial porin in lipid bilayer membranes. Demonstration of voltage gating and of negative point charges at the channel mouth. J. Biol. Chem. *268*, 6234–6240.

Vollrath, M.A., Kwan, K.Y., and Corey, D.P. (2007). The micromachinery of mechanotransduction in hair cells. Annu. Rev. Neurosci. *30*, 339–365.

Wetzel, C., Pifferi, S., Picci, C., Gok, C., Hoffmann, D., Bali, K.K., Lampe, A., Lapatsina, L., Fleischer, R., Smith, E.S.J., et al. (2017). Small-molecule

inhibition of STOML3 oligomerization reverses pathological mechanical hypersensitivity. Nat. Neurosci. *20*, 209–218.

Woo, S.H., Lukacs, V., de Nooij, J.C., Zaytseva, D., Criddle, C.R., Francisco, A., Jessell, T.M., Wilkinson, K.A., and Patapoutian, A. (2015). Piezo2 is the principal mechanotransduction channel for proprioception. Nat. Neurosci. *18*, 1756–1762.

Yang, X.C., and Sachs, F. (1989). Block of stretch-activated ion channels in Xenopus oocytes by gadolinium and calcium ions. Science *243*, 1068–1071.

Zaelzer, C., Hua, P., Prager-Khoutorsky, M., Ciura, S., Voisin, D.L., Liedtke, W., and Bourque, C.W. (2015). ΔN-TRPV1: A Molecular Co-detector of Body Temperature and Osmotic Stress. Cell Rep. *13*, 23–30.

Zeisel, A., Hochgerner, H., Lonnerberg, P., Johnsson, A., Memic, F., van der Zwan, J., Haring, M., Braun, E., Borm, L.E., La Manno, G., et al. (2018). Molecular Architecture of the Mouse Nervous System. Cell *174*, 999–1014.e22.

Zhang, M., Wang, Y., Geng, J., Zhou, S., and Xiao, B. (2019). Mechanically Activated Piezo Channels Mediate Touch and Suppress Acute Mechanical Pain Response in Mice. Cell Rep. *26*, 1419–1431.e4.

STAR★METHODS

KEY RESOURCES TABLE

REAGENT or RESOURCE	SOURCE	IDENTIFIER
Antibodies		
Custom polyclonal antibody against peptide RPSLPSESMEAAQELENQMKERQG of TACAN (aa 68-92)	MediMabs	N/A
Anti-Neurofilament 200 antibody produced in rabbit	Sigma	Cat# N4142; RRID: AB_477272
Monoclonal Anti-Calcitonin Gene-Related Peptide antibody produced in mouse	Sigma	Cat# C7113; RRID: AB_259000
Anti-GINIP	Gaillard et al. (2014)	N/A
Anti-P2X3	Neuromics	Cat# GP10108; RRID: AB_2283325
Anti-Tyrosine Hydroxylase antibody	Abcam	Cat# Ab76442; RRID: AB_1524535
Goat anti-rabbit conjugated to Alexa Fluor 488	ThermoFisher	Cat# A32731; RRID: AB_2633280
Goat anti-mouse conjugated to Alexa Fluor 594	ThermoFisher	Cat# A32742; RRID: AB_2762825
Goat anti-rat conjugated to Alexa Fluor 594	ThermoFisher	Cat# A-11007; RRID: AB_10561522
Goat anti-chicken conjugated to Alexa Fluor 594	ThermoFisher	Cat# A32759; RRID: AB_2762829
Donkey anti-mouse conjugated to Rhodamine Red X	Jackson Immunoresearch	Cat# 715-295-151; RRID: AB_2340832
Isolectin GS-IB4 From Griffonia simplicifolia, Alexa Fluor 594 Conjugate	ThermoFisher	Cat# I21413; RRID: AB_2313921
Anti-HA	Covance	Cat# MMS-101P; RRID: AB_2314672
Beta tubulin Antibody	Novus Biologicals	Cat# NB600-936; RRID: AB_10000656
Peroxidase AffiniPure F(ab')$_2$ Fragment Goat Anti-Mouse IgG (H+L)	Jackson ImmunoResearch	Cat# 115-036-062; RRID: AB_2307346
Peroxidase AffiniPure Goat Anti-Rabbit IgG (H+L)	Jackson ImmunoResearch	Cat# 111-035-144; RRID: AB_2307391
Bacterial and Virus Strains		
scAAV6-GFP-U6-mTMEM120A-shRNA	Vector Biolabs	Cat# 70001, lot 2015-0330,
scAAV6-GFP-U6-scrmb-shRNA	Vector Biolabs	Cat# 77777, lot 2015-0330
Biological Samples		
Human dorsal root ganglia	Transplant Quebec Organ Donation	N/A
Chemicals, Peptides, and Recombinant Proteins		
Tamoxifen	Sigma	Cat# T5668
TRYPSIN	Wisent	Cat# 325-043-EL
COLLAGENASE TYPE I, CLS I	Biochrom	Cat# C 1-28
Dispase II	Sigma	Cat# D4693
Dispase II, powder	ThermoFisher	Cat# 17105041
Collagenase, Type II, powder	ThermoFisher	Cat# 17101015
Trichloro(1H,1H,2H,2H-perfluorooctyl)silane	Sigma	CAS Number: 78560-45-9
GsMTx4	Tocris	Cat# 4912
Critical Commercial Assays		
ViewRNA® ISH Tissue 2-Plex Assay Kit	Affymetrix	Cat# QVT0012
RNAscope® 2.5 LS Duplex Reagent Kit	Advanced Cell Diagnostics	Cat# 322440
RNAscope® 2.5 LS Green Accessory Pack	Advanced Cell Diagnostics	Cat# 322550
RNAscope® LS 2.5 3-plex Positive Control Probe- Hs	Advanced Cell Diagnostics	Cat# 320868
RNAscope® 3-plex LS Multiplex Negative Control Probe	Advanced Cell Diagnostics	Cat# 320878
RNAscope® 2.5 LS Probe- Hs-TMEM120A	Advanced Cell Diagnostics	Cat# 551688
RNAscope® 2.5 LS Probe- Hs-TRPV1-C2	Advanced Cell Diagnostics	Cat# 415388-C2
FuGENE® HD Transfection Reagent	Promega	Cat# E2311
DC Protein Assay Kit I	BIO-RAD	Cat# 5000111

(*Continued on next page*)

Continued

REAGENT or RESOURCE	SOURCE	IDENTIFIER
ReliaPrep RNA Cell Miniprep System Protocol	Promega	Cat# Z6011
Maxima First Strand cDNA Synthesis Kit for RT-qPCR	Thermofisher	Cat# K1641
QuantiNova Probe PCR Kit	QIAGEN	Cat# 208254
Tmem120a probe (Mm00659987_m1)	Thermofisher	Cat# 4331182
Beta actin probe (Mm00607939_s1)	Thermofisher	Cat# 4331182
RNAscope® Fluorescent Multiplex Assay	Advanced Cell Diagnostics	Cat# 320850
RNAscope® Protease III & Protease IV Reagent	Advanced Cell Diagnostics	Cat# 322340
RNAscope® 3-plex Positive Control Probe- Mm	Advanced Cell Diagnostics	Cat# 320881
RNAscope® 3-plex Negative Control Probe	Advanced Cell Diagnostics	Cat# 320871
RNAscope® Fluorescent Multiplex Detection Reagents	Advanced Cell Diagnostics	Cat# 320851
RNAscope® Probe- Mm-Tmem120a	Advanced Cell Diagnostics	Cat# 513211
RNAscope® Probe- Mm-P2rx3	Advanced Cell Diagnostics	Cat# 511611-C2
ACD HybEZ oven (ACD cat 241000)	Advanced Cell Diagnostics	Cat# 241000
Experimental Models: Cell Lines		
COS-7	ATCC	Cat# CRL-1651
HEK293 (tsa201)	Sigma	Cat# tsa201
Piezo1 KO	Dr. A. Patapoutian, Scripps Research Institute	N/A
CHO cell line stably expressing TACAN-HA	This paper	N/A
Rosetta(DE3)pLysS Competent Cells	Sigma	Cat# 70956
Neuro-2a	ATCC	Cat# CC-L131
Experimental Models: Organisms/Strains		
C57BL/6 mice	Jackson Laboratories	Cat# 000664
TRPV1-cre mice	Jackson Laboratories	Cat# 017769
Gt(ROSA)26Sor$^{tm9(CAG-tdTomato)Hze}$/J	Jackson Laboratories	Cat# 007909
Mrgprd^{CreERT2}	Jackson Laboratories	Cat# 031286
F11	ECACC	Cat# 08062601
Oligonucleotides		
(QIAGEN FlexiTube siRNA final concentration 100nM, #Mm MGI:2686991.1)	QIAGEN	N/A
AllStars Neg. siRNA AF 488 (5 nmol)	QIAGEN	Cat# 1027284
Software and Algorithms		
MATLAB 9.1 (R2016b)	MathWorks	https://www.mathworks.com
Clampex10	Molecular Devices	N/A
MetaMorph Advanced software	Molecular Devices	N/A
GPatch software suite	UCLA Department of Anesthesiology	N/A
Analysis Software	UCLA Department of Anesthesiology	N/A
Mascot version 2.3.01	Matrix Science	http://www.matrixscience.com/
Scaffold 4.8.2	Proteome Software	http://www.proteomesoftware.com/products/scaffold/
Other		
μ-Dish 35 mm, low	Ibidi	Cat# 80136
HBSS, 1X	Wisent	Cat# 311-511-CL
Tissue-Tek* O.C.T. Compound	VWR	Cat# 4583
INNOVEX BIOSCIENCES ADVANTAGE MOUNTING MEDIA	Innovex	Cat# NB300
NeuroTrace 530/615 Red Fluorescent Nissl Stain - Solution in DMSO	ThermoFisher	Cat# N21482
Aqua-Poly/Mount	Polysciences Inc	Cat# 18606-20
FluoroDish Cell Culture Dish - 35mm, 10mm well, pkg of 100	World Precision Instruments	Cat# FD3510-100

(*Continued on next page*)

Continued

REAGENT or RESOURCE	SOURCE	IDENTIFIER
MultiClamp 700B	Axon Instruments	N/A
Digidata 1440A	Molecular Devices	N/A
High Speed Pressure Clamp	ALA Scientific	Cat# HSPC
CCD camera	QI maging	Cat# QI Click
Neurobasal Medium	ThermoFisher	Cat# 21103049
BURLEIGH PZ-150M PIEZO DRIVER/AMPLIFIER	AssetRelay	N/A
Sylgard 184	Sigma	Cat# 761036
ZEPTO LOW COST PLASMA LABORATORY UNIT	Diener	N/A
P-1000 Next Generation Micropipette Puller	Sutter Instruments	Cat# P-1000
Micromanipulator	Kleindiek	Cat# MM3A-LS
Perfusion Fast-Step Translator	Warner	Cat# SF-77C
Axopatch 200A	Axon Instruments	N/A
cOmplete, Mini, EDTA-free Protease Inhibitor Cocktail	Sigma	Cat# 11836170001
AVESTIN EMULSIFLEX C5	ATA Scientific	N/A
MAPCHO®-14	Sigma	Cat# 850338P
EZ-Link Sulfo-NHS-SS-Biotin	ThermoFisher	Cat# 21331
Pierce NeutrAvidin Agarose	ThermoFisher	Cat# 29200
Immobilon-P PVDF Membrane	Sigma	Cat# IPVH00010
ProLong Gold Antifade Mountant	Thermofisher	Cat# P36930
Fisherbrand Superfrost Plus Microscope Slides	Fisher scientific	Cat# 12-550-15

LEAD CONTACT AND MATERIALS AVAILABILITY

Further information and requests for resources and reagents should be directed to and will be fulfilled by the Lead Contact, Reza Sharif-Naeini (reza.sharif@mcgill.ca). This study did not generate new unique reagents.

EXPERIMENTAL MODEL AND SUBJECT DETAILS

C57BL/6 Mice

Adult male C57BL/6 mice (8-12 weeks old, Jackson Laboratories) were housed in a temperature-controlled room under a 12h light/dark cycle. Water and food were available *ad libitum*.

Trpv1-tdTom mice

TRPV1-cre mice (B6.129-*Trpv1*$^{tm1(cre)Bbm}$/J, Stock #017769) were crossed to the tdTomato (tdTom) reporter line B6.Cg-Gt(ROSA)26Sor$^{tm9(CAG-tdTomato)Hze}$/J (B6.129-*Gt(ROSA)26Sor*^{tm1Joe}/J, Stock # 007909) to produce mice in which nociceptors express tdTomato (termed *Trpv1-tdTom*). Mice expressing an inducible Cre recombinase in non-peptidergic nociceptors Mrgprd^{CreERT2} were obtained from Dr. Wenqin Luo (Jackson labs stock #031286) and crossed to TACAN floxed mice, in which loxP sites were introduced upstream of exon 2 and downstream of exon 3. Tamoxifen (Sigma #T5668; 100mg + 0.5ml EtOH 100% + 9.5ml sunflower oil (Sigma), sonicated 45 min, and stored at −20°C for a maximum of 1 month) was prepared in a 10 mg/ml solution and injected twice daily for 5 days at 50mg/kg.

Human dorsal root ganglia

Collection of human dorsal root ganglia was approved by the ethical review board at McGill University (IRB#s A04-M53-08B) in collaboration with Transplant Quebec Organ Donation. After receiving appropriate consent, DRGs were collected in NMDG-aCSF following thoracolumbar spine harvest (T10/11 to L5/S1) no longer than 3 hours after aortic cross-clamp. The donor was a 68 year old male who died of stroke, without any history of chronic pain.

COS7 cells

COS7 (ATCC, #CRL-1651) or HEK293 (tsA201) (a gift from Dr. D. Bowie, McGill University) cells were grown in 35mm dishes to 70%–80% confluency and transfected with a bicistronic vector expressing TACAN-HA and EGFP (or empty EGFP control vector) using FuGene HD transfection reagent (Promega, #E2311). On the following day, cells were split at low confluency (5%–10%) on 35mm tissue culture treated μ-dishes (Ibidi, #80136). Electrophysiology recordings were done 48 to 72 h post-transfection.

Piezo1 KO cells

Piezo1 KO HEK293 cells were obtained from the lab of Dr. A. Patapoutian, Scripps Research Institute.

Stable CHO cell generation

CHO cells were transfected with a P2A bicistronic vector simultaneously expressing (N-terminal) HA-tagged human TACAN and nuclear TdTomato (pCMV-NLS-tdTom-P2A-2HA-TACAN = HA-TACAN), or with a control vector expressing nuclear TdTomato alone (pCMV-NLS-tdTom-P2A-2HA = MOCK). Selection media supplied with 800 μg/mL G418 was added 24h post-transfection. On the second day post-transfection, the cells were plated at high dilution (1:150) in 10 cm dishes. One week post transfection, a total of eight colonies were collected and grown in separate dishes. Expression levels of TACAN protein were measured for each clone by western blot using an anti-HA antibody.

Mouse DRG culture

DRGs from 8-12 week old male mice were dissected, dissociated and cultured as follows: freshly dissected DRGs were initially stored in Hank's Balanced Salt Solution (HBSS, Wisent, #311-511-CL), then enzymatically dissociated by incubating first with 0.25% trypsin-EDTA (Wisent, #325-043-EL) for 20 minutes at 37°C, then with collagenase type I (Biochrom, # C 1-28; 2 mg/ml) and dispase II protease (Sigma, #D4693; 5 mg/ml) in HBSS for 30-40 minutes at 37°C. The suspension was centrifuged for 2 minutes at 800 rpm, the enzymatic solution was removed and replaced with 200 μl of DRG culture media (for composition, see Hu and Lewin, 2006). DRG neurons were mechanically separated by trituration and plated on poly-L-lysine- (100 μg/ml) and laminin- (20 μg/ml) coated 35 mm glass-bottom FluoroDishes (World Precision Instruments Inc., #FD3510-100) and incubated at 37°C.

METHOD DETAILS

In Situ Hybridization

Mouse DRG

We used the ViewRNA ISH assay from Affymetrix (Affymetrix eBioscience # QVT0012) according to the manufacturer's protocol. Briefly, freshly dissected DRGs were embedded in an optimum cutting temperature medium (Tissue Tek, O.C.T. Compound, #4583) and placed on dry ice. 14 μm thick sections were cut on a cryostat (Leica, Germany) at −20°C, mounted onto slides and fixed in 10% normal buffer formalin overnight. The tissue was dehydrated, baked and digested for 20 minutes with Protease QF. Following protease treatment, the sections were incubated for 3h at 40°C with a target probe set designed to hybridize with mouse TACAN (accession number #NM_172541) or with no target probe added for the negative control slides. The signal was amplified through sequential hybridization with preamplifier and amplifier mixes and revealed by hybridization with label probe oligonucleotides conjugated to alkaline phosphatase and precipitation of Fast Red Substrate. Finally, the sections were stained with DAPI, counterstained with Gill's hematoxylin and mounted using Advantage Mounting Medium (Innovex Biosciences Inc, # NB300).

Human DRG

The RNAscope® LS Duplex Assay (Red/Green) (322440, 322550), purchased from Advanced Cell Diagnostics (ACD, a Bio-Techne brand), was performed at the MIRC Core Histology Facility (Hamilton, ON) on a Leica Bond RX. Ganglia were prepared according to the manufacturer's protocol for Fresh Frozen samples and sectioned to 14 μm prior to staining. Sample RNA quality and background staining were assessed with positive (320868) and negative control probes (320878). Target staining was performed with probes for TMEM120A (551688) and TRPV1 (415388-C2). Counterstaining was performed with Gill's Hematoxylin I and slides were mounted with Vectamount.

P2X3

The mRNA TACAN and P2X3 were analyzed from slides of fresh frozen sections from WT and MrgdCre x Tacan flox (Tamoxifen treated) brains fixed for 15 minutes in cold 4% PFA (prepared in 1xPBS) using the advanced cell diagnostics RNAscope fluorescent multiplex reagent kit (ACD, Newark,USA, cat# 320850). After fixation, the sections were dehydrated in ethanol and pretreated with Protease IV (ACD cat 322340, lot 2006478) at room temperature for 30 minutes. Pretreated sections were incubated for 2 hours at 40°C in ACD HybEZ oven (ACD cat# 241000) with RNAscope probes against TACAN (Mm Tmem120a – C1, ACD reference 513211, lot 19066C) and P2X3 (Mm P2rx3 – C2, ACD ref 521611-C2, lot 19101D). Control slides were treated with a mouse Positive Control Probe (ACD ref 320881, lot 19099A) and 3-Plex negative control probe (ACD ref 320871, lot 19162A). The signal was amplified through a series of three sequential hybridization steps using amplification reagents included in the Fluorescent Multiplex Detection Reagents Kit (cat 320851, lot 2006207). The final amplification reagent (Amp 4-FL-Alt C) included fluorophores Atto 647 (revealing P2X3) and Atto 550 (revealing TACAN). Finally, the sections were stained with DAPI and mounted using ProLong Gold antifade reagent (Invitrogen, ref P36930, lot 2046607) on Fisherbrand Superfrost Plus Microscope Slides (cat 12-550-15).

Generation of an affinity-purified rabbit antibody against TACAN

A custom polyclonal antibody against peptide RPSLPSESMEAAQELENQMKERQG (aa 68-92) was produced in rabbit by standard methods (MediMabs). TACAN antibody was affinity purified by incubating the serum with an antigen peptide bound to a PVDF membrane (prepared based on the pMAL Protein Fusion and Purification System, New England Biolabs).

Immunohistochemistry

To determine which population of sensory fibers expresses TACAN in mice, DRGs were processed for immunohistochemistry using antibodies against TACAN in combination with those against either NF200, CGRP, GINIP, P2X3 and TH to label myelinated fibers, peptidergic sensory fibers, non-peptidergic fibers, and two subpopulations of non-peptidergic fibers: MRGPRD nociceptors and C-low threshold mechanoreceptors (C-LTMRs), respectively. The lectin IB4 was used to identify non-peptidergic sensory fibers and Nissl stain was used to label cell bodies of DRG neurons. DRGs were embedded in O.C.T. and 14-μm thick sections were cut on a cryostat (Leica, Germany) at −20°C and slide mounted directly. All sections were washed for 30 min with PBS containing 0.2% Triton-X (PBS-T), incubated in 50% ethanol for 30 min and washed in PBS-T. Depending on the species in which the secondary antibody was raised in, the tissue was either blocked in 10% normal donkey or normal goat serum for 1 h. Primary antibodies were used at the following concentrations – anti-TACAN (1:1000; rabbit polyclonal, affinity purified, MediMabs), anti-NF200 (1:1000, mouse polyclonal, Sigma, #N4142), anti-CGRP (1:1000, mouse monoclonal, Sigma, #C7113), anti-GINIP (1:1000, rat polyclonal, a gift from Dr. Aziz Moqrich; Gaillard et al., 2014), anti-P2X3 (1:5000, guinea pig polyclonal, Neuromics, #GP10108), anti-TH (1:250, chicken polyclonal, Abcam, #ab76442), and IB4 conjugated to Alexa Fluor 594 (1:200, ThermoFisher Scientific) made in 5% blocking serum (goat or donkey) in PBS-T and left to incubate overnight on the shaker at 4°C. To test for anti-TACAN specificity, DRG sections were co-incubated with the synthetic blocking peptide (1:200; MediMabs). Following 30 min of washes with PBS-T, the tissue was incubated with the appropriate secondary antibody diluted in PBS-T for 2 h at room temperature– goat anti-rabbit conjugated to Alexa Fluor 488 (1:800, ThermoFisher Scientific), goat anti-mouse conjugated to Alexa Fluor 594 (1:800, ThermoFisher Scientific), goat anti-rat conjugated to Alexa Fluor 594 (1:500, ThermoFisher Scientific), goat anti-chicken conjugated to Alexa Fluor 594 (1:100, ThermoFisher Scientific), or donkey anti-mouse conjugated to Rhodamine Red X (1:200, Jackson Immunoresearch). To label all DRG neurons, sections were incubated with the red fluorescent Nissl stain NeuroTrace 530/615 (1:200, ThermoFischer #N21482) for 20 min at room temperature. Following 30 min of washes, all slides were mounted with Aqua-Poly/Mount (Polysciences Inc., #18606-20).

Representative images were taken using a Zeiss LSM510 confocal microscope equipped with Ar and He-Ne lasers using a 20x water-immersion objectives. Images used for quantifications were taken on a Zeiss Axio Imager M2 fluorescence photomicroscope (Zeiss Canada) using a 10x objective.

Cell-attached recordings

Extracellular neuronal bath solution (pH 7.40 and 303 mOsm) consisted of (in mM): NaCl 140, KCl 5, $CaCl_2$ 2, $MgCl_2$ 2, HEPES 10, and Glucose 10. For whole-cell and outside-out recordings, the electrode contained a solution (pH 7.20 and 302 mOsm) consisting of (in mM): K-Gluconate 123, KCl 10, $MgCl_2$ 1, HEPES 10, EGTA 1, $CaCl_2$ 0.1, K_2ATP 1, Na_4ATP 0.2, and Glucose 4. For cell-attached recordings, the recording electrode was filled with the same solution as the extracellular neuronal bath. Electrodes were made using fire-polished glass electrodes (AM Systems, Glass Borosilicate, 1.5 mm OD, 0.86 ID) with resistances of 1.5-2 MOhms (cell-attached), 1.5-3.5 MOhms (outside-out), and 4-8 MOhms (whole-cell).

Observations were made on Olympus IX71 inverted microscope with a MultiClamp 700B (Axon CNS, Molecular Devices, Sunnyvale, CA, USA) as amplifier and Digidata 1440A (Molecular Devices) as digitizer. Membrane current and voltage were amplified and acquired via the MultiClamp and Digidata and were sampled at 10 kHz; signals were recorded with Clampex10 and MultiClamp 700B software. In whole-cell recordings, pipette and membrane capacitance were compensated for with the auto function of Clampex10. The electrode holder was connected to a high-speed pressure clamp and Pressure-Vacuum pump (HSPC, ALA Scientific) for pressure-pulse recording protocols, such that pressure stimuli were delivered directly through the recording electrode, as previously described (Peyronnet et al., 2012). Mechanical stimulation protocols were written in Clampex10, and performed by the HSPC, with less than a 10ms rise time from no applied pressure to intended magnitude of pressure. The threshold amplitude for accepting an opening event was set at 50%. The minimum duration of open events was set at 100 μs, in concordance with previous standards (Cho et al., 2002). For the majority of cell-attached recordings, membrane voltage was held at −80 mV to generate more discernable mechanically evoked channel openings. Each cell membrane patch was subjected to 11 sweeps of incrementally increasing negative pressure from 0 mm Hg to −100 mm Hg, at 10 mm Hg increments. Images of cell soma were taken at 40X with a CCD camera (QImaging, QI Click) connected to the microscope. Images were saved and analyzed with Olympus MetaMorph Advanced software.

Whole-cell recordings with mechanical stimulation via cell indentations

Mouse DRG cultures were prepared as previously described (Francois et al., 2015). Briefly, male adult mice (8-12 weeks) were anesthetized and perfused with cold HBSS. DRG were removed and enzymatically digested with 5 mg/ml dispase (ThermoFisher Scientific #17105041) and 2 mg/ml collagenase II (Thermo Fisher Scientific #17101-015) at 37°C for 40 minutes. DRGs were then rinsed with Neuro Basal A media (Thermo Fisher Scientific #21103049) with B27 supplement, 2 mM L-glutamine and 100 mg/ml penicillin-streptomycin. After mechanical dissociation with syringes of decreasing diameter (18 G, 21 G and 26 G), neurons were plated on 35 mm dishes (Ibidi #80136) previously coated with Poly-L-ornithine and laminin. One hour later, media was replaced by complete Neuro Basal A media (with growth factors: 10 ng/ml NT4, 2 ng/ml GDNF and 200 ng/mL NGF; ThermoFisher). 72 hours after transfection with siRNA (see TACAN knockdown section below), whole-cell patch clamp was performed on Alexa 488 and IB4 (anti IB4-Alexa 594 1/2000, Thermo Fisher Scientific #I21413) positive neurons. The extracellular solution contained (in mM): 10 glucose, 140 NaCl, 4 KCl, 2 $MgCl_2$, 10 HEPES, 2 $CaCl_2$, pH 7.30. The pipette solution contained (in mM): 127 K-Gluconate, 10 NaCl, 5 KCl,

4 Mg-ATP, 0.4 Na-GTP, 5 Creatine P (Na), 1 $CaCl_2$, 10 EGTA, 1 $MgCl_2$, 10 HEPES, pH 7.20. Cells were patched in the voltage-clamp whole-cell configuration, maintained at −60 mV, and mechanically stimulated with a blunt glass pipette attached to a piezo-electric device (PZ-150 M; Burleigh) as previously described (Francois et al., 2015). Cells were stimulated during 2 s with increasing indentation steps of 1 μm at two speeds: 80 and 800 μm/s for slow and fast stimulation, respectively during the ramp segment of the command for both forward and backward motions. The time constants of MS current decay were fitted to exponentials as in Delfini et al. (2013). These descriptors were used to classify the proportion of different mechanically-activated current adaptations in rapidly, mixed and slowly adapting categories.

Whole-cell recordings with mechanical stimulation via micropillar substrate deflection

Micropillar array fabrication

Positive masters and pillar array casting were described previously (Poole et al., 2014; Sianati et al., 2019). Briefly, negative masters were cast in polydimethylsiloxane (PDMS) (Sylgard 184, Dow Corning, mixed at a ratio of 1:10, cured at 110°C for 15 min) from positive silicon masters silanised with vapor phase Trichloro (1H,1H,2H,2H-perfluorooctyl) silane (Sigma-Alrich). Negative masters were then silanised (as above) and used to cast pillar arrays, also in PDMS, ratio 1:10, cured at 110°C for 60 min. Before seeding cells (Piezo1-knockout cells with or without transfected TACAN), pillar arrays were activated using a low pressure Zepto plasma system (Diener, Germany). Cells were seeded at a concentration of 2×10^4 cells/mL in complete media, transiently transfected using Fugene HD (as per manufacturer's instructions) and incubated overnight.

Electrophysiology

Whole-cell patch pipettes were prepared from thick-walled filamented glass using a pipette puller fitted with a box filament (P-1000, Sutter Instruments, USA). Pipettes were heat-polished to give a final resistance of 3 MΩ – 6 MΩ, and filled with a solution containing 110 mM KCl, 10 mM NaCl, 1 mM $MgCl_2$, 1 mM EGTA and 10 mM HEPES (pH 7.3). Extracellular solutions contained 140 mM NaCl, 4 mM KCl, 2 mM $CaCl_2$, 1 mM $MgCl_2$, 4 mM glucose and 10 mM HEPES (pH 7.4). Whole-cell patch-clamp data was obtained on an Axopatch 200B with pClamp 10 software. Data were analyzed using Clampfit software (Molecular Devices, USA). Pipette and membrane capacitance were compensated and to minimize voltage errors, series resistance was compensated by at least 60%. Mechanically-activated currents were recorded at a holding potential of −60 mV. Multiple mechanical stimuli ranging between 1 nm–1 μm were applied to cells by serially deflecting an individual pilus using a blunt, heat-polished pipette driven by a MM3A-LS micromanipulator (Kleindiek Nanotechnik, Germany). Bright-field images of the deflected pilus were collected with a Nikon T*i*-E inverted microscope using a 40 × objective (NA 0.6) and the center of each pilus was calculated off line by applying a 2D-Gaussian fit of intensity values (Igor, Wavemetrics, USA). Pillar deflection was subsequently calculated from successive images by comparing the difference in the calculated center point.

Outside-out recordings and GsMTx4 treatment

For outside-out recordings, patches were subjected to incrementally increasing levels of positive pressure until they reached a threshold opening (with pressure increments of 5 mm Hg). Once threshold was reached, the patch was subjected to that threshold pressure for 10 sweeps. Superfusion through a fast solution exchanger (SF-77B, Warner Instruments) was set-up in the dish so that a constant stream of external bath solution or 5μM GsMTx4 dissolved in external bath solution was directed toward the recording electrode, with the perfusion line ~2 mm away from the electrode. An initial 10-sweep pressure pulse protocol was performed in the presence of external bath solution. Following ~30 s of GsMTx4 perfusion (to allow for adequate GsMTx4 insertion into the membrane), another 10-sweep protocol was performed. Finally, 5-10 minutes after wash with external bath solution, a 10-sweep protocol was performed on the same outside-out patch. GsMTx-4 is a 34-residue peptide extracted from the *Grammostola spatulata* tarantula toxin that blocks stretch-activated ion channels (Chen et al., 1996), and was purchased commercially (Tocris cat. #4912). The peptide was dissolved in saline in stocks of 50μM and stored at −80°C.

Bilayer recordings

Bilayers were formed in polyethylene chips featuring a 150μm diameter aperture by brushing a solution of 10mg/ml Di-phitanoyl-phosphatidylcholine (DPhPC) diluted in decane over the aperture. We exclusively used synthetic lipids to prevent any contamination with other proteins from a lipid purification process. Thinning of the bilayer was monitored via membrane capacitance.

TACAN channels were reconstituted by mixing POPE:POPG (3:1) small unilamellar vesicles with the purified channels in solution (1:4 by weight protein:lipid), and removing the detergent by dialysis over 5 days as described previously (Faure et al., 2012). Channels were fused by adding 1μl of the proteoliposome suspension to one chamber and monitoring fusion by current increase. Electrophysiological recording was performed with an Axopatch 200A amplifier and the GPatch software suite (UCLA Department of Anesthesiology). Currents were analyzed using Analysis Software (UCLA Department of Anesthesiology). For macroscopic currents, we used solutions containing in mM, *cis*: 150 NaCl, 10 HEPES (pH 7.40) and trans: 150 KCl, 10 HEPES, (pH 7.40). For single-channel recordings, we used used solutions containing in mM, *cis*: 500 NaCl, 10 HEPES (pH 7.40) and trans: 500 KCl, 10 HEPES, (pH 7.40).

TACAN purification

For reconstitution in artificial bilayers, human TACAN was inserted into a pET28a vector, with a N-terminal His tag (6x) followed by a thrombin cleavage site. TACAN-pET28a was transformed into *E. coli* DE3-pLys (Rosetta) competent cells. 100mL of pre-culture was

grown overnight in LB medium supplemented with 50μg/mL kanamycin at 37°C in an incubator shaking at a speed of 240 rpm. 1-4L of culture was inoculated with 10mL of pre-culture. Once OD 0.8 was reached (> 3h), IPTG (final concentration of 0.5 mM) and glycerol 50mL/L culture (∼5%) were added to induce TACAN expression. Best induction was achieved at 20°C for > 5hrs (Figure S6A). Cells were harvested by centrifuging cultures at ∼4000 g for 15 min at 4°C. Pellets were pooled, washed once and resuspended at a concentration of 1/7 g/mL with resuspension buffer (0.5 M NaCl, 50 mM HEPES, 10% glycerol, pH adjusted to 7.50 with KOH) containing 1 pellet of protease inhibitor (mini complete EDTA-free, Sigma #11836170001). The suspension was kept on ice at all times.

After homogeneous resuspension by agitation, the cells were lysed by passing through a cell disrupter (Emulsiflex C5, Avestin, Ottawa) 3 times at 15,000psi. Unbroken cells and debris were subsequently removed by centrifugation at 18,000 g for 15min at 4°C. The supernatant was ultra-centrifuged at 160,000 g for 2h at 4°C and the pellet (membranes) was collected. Membranes were resuspended in 2mL/L of culture IMAC-buffer (0.5 M NaCl, 20 mM HEPES, 10 mM imidazole, 10% glycerol, 0.02% Fos-choline-14, pH adjusted to 7.50 with KOH), transferred into a homogenizer and homogenized mechanically. Fos-choline-14 (2%, Avanti) was added and agitated for 2h at 4°C. Non-soluble debris was removed by centrifugation at 100,000 g for 30 min.

Proteins were bound to Co-resin (Talon superflow) and washed with 25mM imidazole in a FPLC (Äkta purifier). Following a careful wash in the presence of 25 mM imidazole, the protein was eluted at 400 mM imidazole and concentrated. TACAN was further purified by size-exclusion. The sample was passed through a G75 column (buffer: 0.5 M NaCl, 20 mM HEPES, 5% glycerol, 0.02% Fos-choline-14, pH adjusted to 7.50 with KOH). TACAN was collected at the 9.2ml fraction. Purity and size were confirmed by western blot (Figure S6A).

Mass Spectrometry of purified TACAN

Purified TACAN was digested with trypsin and analyzed by tandem MS/MS (see table S2). All MS/MS samples were analyzed using Mascot (Matrix Science, London, UK; version 2.3.01). Mascot was set up to search the MiscService_02_May_2014_10_05_42 database (unknown version, 21 entries) assuming the digestion enzyme trypsin. Mascot was searched with a fragment ion mass tolerance of 0.50 Da and a parent ion tolerance of 15 PPM. Deamidation of asparagine and glutamine, oxidation of methionine, carbamidomethylation of cysteine and phosphorylation of serine, threonine and tyrosine were specified in Mascot as variable modifications.

Scaffold (version Scaffold_4.8.2, Proteome Software Inc., Portland, OR) was used to validate MS/MS based peptide and protein identifications. Peptide identifications were accepted if they could be established at a probability greater than 95.0% by the Peptide Prophet algorithm (Keller et al., 2002) with Scaffold delta-mass correction. Protein identifications were accepted if they could be established at a probability greater than 99.0% and contained at least 1 identified peptide. Protein probabilities were assigned by the Protein Prophet algorithm (Nesvizhskii et al., 2003). Proteins that contained similar peptides and could not be differentiated based on MS/MS analysis alone were grouped to satisfy the principles of parsimony. TACAN was identified by 130/376 amino acids (35% coverage) and no decoys were identified (Figure S6B).

CHO HA-TACAN membrane staining and imaging

CHO cells stably expressing HA-TACAN (and TdTomato) were grown in alpha-MEM supplemented with 10% FBS, 1% Pen/Strep and 400 μg/mL (0.8mM) G418. At P17, they were trypsinized, plated on Poly-D-Lysine-coated glass coverslips and incubated for 24 h.

CHO cells were incubated in DiI (1:200 in their respective media) for 10 min at 37°C. Following DiI staining, they were fixed in 4% paraformaldehyde for 20 min at 4°C. They were then incubated in 0.5% tritonX for 20 min to permeabilize the membranes. Next, they were blocked in 10% NGST for 1h at room temperature. Incubation with an anti-HA rabbit polyclonal antibody (1:2000 in NGST; Invitrogen #71-5500) took place overnight at 4°C. The next day, the cells were incubated with an AlexaFluor-488 goat anti-rabbit antibody (1:500 in NGST) for 1 h at room temperature. Finally, the coverslips were mounted on glass slides for imaging. All dilutions were done in PBS unless otherwise indicated, and cells were rinsed with PBS 2-3 times after each step except for the blocking step.

Images were collected using a Zeiss LSM 710 confocal microscope with a 63x oil objective. A focal plane through the center of the cell was selected based on the DiI staining of the membrane. The stably transfected CHO cells were identified by their nuclear tdTomato signal. All analysis was done using ImageJ. First, a mask was created from the red channel by thresholding the image, converting to binary, getting an outline of the cell and inverting the image such that the membrane, as defined by the DiI staining, appeared as a one-pixel thick outline. Black pixels that were clearly not part of the membrane were manually erased using the paintbrush tool. The resulting image was subtracted from the green channel so that only the HA signal at the membrane remained. A free-hand ROI was drawn around each cell of interest such that it encompassed the entire membrane of the cell. The values of the pixel intensity within this ROI were extracted and an average overall nonzero pixel intensity was taken to determine the average intensity of pixels around the membrane.

Biotinylation on CHO stable cell line

CHO stable cell lines (MOCK and HA-TACAN = TACAN) were grown on 60mm dishes to 70% confluency. Briefly, the cells were washed with ice cold PBS-CM and incubated for 30 minutes on ice, in the dark with a 0.5 mg/ml sulfo-NHS-SS-biotin (Thermo-Scientific, #21331) diluted in PBS-CM pH 8.0. The biotinylation reaction was stopped by quenching with 50 mM glycine diluted in PBS-CM and the cells were lysed in 250 μL RIPA lysis buffer. The cells were harvested by scraping and collected in micro-centrifuge tubes. The lysates were incubated on a rocker at 4°C for 1h. After 20 min of centrifugation at 12,000 g, the supernatant was collected and protein concentration measured according to the Bio-Rad DC Protein Assay Kit I (# 5000111). Equal protein amounts of

each sample were incubated overnight at 4°C with Neutravidin Agarose Resin (Thermo-Scientific, #29200). The following day, the resin was washed four times in RIPA buffer and bound proteins were denatured in Laemmli – 0.1M DTT. Biotinylated samples and cell lysates were loaded on 10% SDS-polyacrylamide gels and transferred to PVDF membranes (Millipore Immobilon, #IPVH00010). Western blot was performed by blocking the membranes in 5% skim milk-PBS and subsequently incubating for 4h at room temperature with 1:2000 mouse anti-HA (Covance #MMS-101P) and 1:8000 anti beta-tubulin rabbit (Novus Biologicals #NB600-936) followed by secondary HRP-conjugated antibodies 1:10 000 (Jackson Immuno Research, #115-036-062 and #111-035-144) for 1 h.

Knockdown of TACAN *in vitro* and *in vivo*

DRG cultures were grown on 35 mm dishes. On the 3rd day, they were treated with complexes of predesigned siRNA directed against mouse TACAN (QIAGEN FlexiTube siRNA final concentration 100nM, #Mm MGI:2686991.1) and 2ul of HiPerFect transfection reagent. The cells were incubated with the transfection complexes for 48 to 72 hours with addition of fresh media 24 h post-transfection.

For *in vivo* knockdown of TACAN, mice were anesthetized with isoflurane and the left sciatic nerve bundle was surgically exposed. We injected two 1 μL doses of a self-complementary adeno-associated virus (sc-AAV, serotype 6, Vector Biolabs) expressing CMV-GFP and U6-shRNA targeting mouse TACAN (genome copies: $1.6x10^{12}$ GC/mL; GenBank RefSeq: NM_172541) or a non-targeting control (genome copies: $1.0x10^{12}$ GC/mL). The injection was performed using a graduated 5 μL PCR glass micropipette (Drummond®) pulled to a fine point. The two viral doses were injected in two different sites on the nerve bundle and the pipette was pulled after 2 min. Skin was sutured using silk suture (PERMA-HAND) and the animal was monitored for an hour after waking to ensure proper mobility.

shRNA sequence:

CCGGTTCCTGCTGGTCTGGTATTATCTCGAGATAATACCAGACCAGCAGGAATTTTTG
Targeting sequence: TTCCTGCTGGTCTGGATTAT
Hairpin loop sequence: CTCGAC
TTTTT terminates shRNA expression for U6 promoter

To validate the knockdown, Neuro2A (N2A) cells treated with siRNA and F11 cells treated with shRNA were studied using qPCR analysis. N2A cells (ATCC catalog #CCL-131) were grown to 50% confluency (in EMEM, 10%FBS, 1% Pen/Strep) on 35 mm dishes and treated for 48h using different concentrations (5nM, 10nM or 20nM) of siRNA directed against mouse TACAN (QIAGEN FlexiTube siRNA, # SI01311919, name Mm_MGI:2686991_1) or 10 nM negative control siRNA (QIAGEN # 1027284). Total RNA was extracted using Promega Relia Prep RNA cell system (#Z6011) and converted to cDNA using Thermo-Fisher Scientific Maxima First Strand cDNA Synthesis kit (catalog #K1641). For each sample, qPCR reactions were performed in quadruplicates on an Applied Biosystems Step One Plus Real Time qPCR System using QIAGEN QuantiNova Probe PCR Kit (QIAGEN #208254) and Taqman Gene expression primer probe mix for mouse TACAN (Thermo-Fisher Scientific Gene Expression Assay number Mm00659987_m1). TACAN gene expression levels were quantified by the double delta Ct analysis using Beta actin (Mm00607939_s1) as a housekeeping reference gene. Results are expressed as means of three independent experiments.

F11 cells (ECACC #08062601) were grown in DMEM + 2mM Glutamine, +2% FBS, +1% Pen/Strep. Cells (passages 15 to 22) were plated in 35 mm dishes at 25% confluency in 1mL of culture medium. Two microliters of viral solution were added the day after plating. Total RNA was extracted 72h after infection when cells had reached about 90% confluency. Three independent experiments were conducted, each experiment consisting of 3 dishes per condition. Expression levels of TACAN were determined by qPCR in quadruplicates as described above.

Von Frey filament test

Animals were placed on a wire-mesh platform in clear plastic cylinders and were allowed to settle for 45 min. Testing was carried out with von Frey filaments of increasing stiffness (from 0.04 to 4g) applied to the plantar surface of the hind paw. One trial consisted of 5 applications of the filament within a one-minute period. The examiner was blind to the animals' genotype or AAV injection during the experiment. Behavioral responses were scored as previously described (Ducourneau et al., 2014), but adapted to mice. Briefly, the mouse reaction to the von Frey application was scored as follows: 0 = no response; 1 = detection (mouse would move its toes or contract its leg muscles without any movement); 2 = withdrawal reaction; 3 = escape (mouse withdraws and avoids further contact with the stimulus by moving its body away from the filament or by guarding its paw); 4 = licking/biting of the stimulated paw after withdrawal. Scores with values higher than 2 were classified as nocifensive reactions. To determine the proportions of responses as below threshold (Figure 6), scores with values of 0 or 1 were pooled together in the ''below threshold'' group. Scores with values of 2 were used in the ''withdrawal reflex'' group, and values of 3 and 4 were pooled together in the ''nocifensive response'' group.

Hargreaves plantar test

Mice were placed on a glass surface in clear plastic cylinders and were allowed to settle for 45min. Radiant heat was delivered from below the glass plate by a heat source (IITC) focused on the hindpaw. The latency to paw withdrawal was measured and averaged for

each trial that consisted of 5 stimulations taken at 5 to 10 min intervals. To avoid tissue damage, a cut-off latency was defined at 30 s (Hargreaves et al., 1988).

Pinprick test

Animals were placed on a wire-mesh platform in clear plastic cylinders and were allowed to settle for 45 min. Pinprick was assessed using a blunted 25G needle gently applied to the plantar surface of the hindpaw five times, without penetration of the skin. The average number of withdrawals induced by the five applications was calculated.

QUANTIFICATION AND STATISTICAL ANALYSIS

Analysis of mechanically-evoked current in cell-attached and outside-out recordings was performed using ClampFit. Traces were baseline-subtracted before setting cursors at the onset and offset of the pressure steps. Statistics were run on the region bounded by these cursors, where we extracted the average current. Some representative traces (when indicated) were also low-pass filtered at 1kHz to better display single-channel openings, and as such, show a smaller background noise level. Mean open time for outside-out recordings was measured on every opening validated by our selection protocol.

Statistical analysis was performed in MATLAB and Excel. Statistical details can be found in the figure legends and in the main text. Reported n values can be found in the figure legends and in the results.

DATA AND CODE AVAILABILITY

This study did not generate any unique datasets or code.

Cell

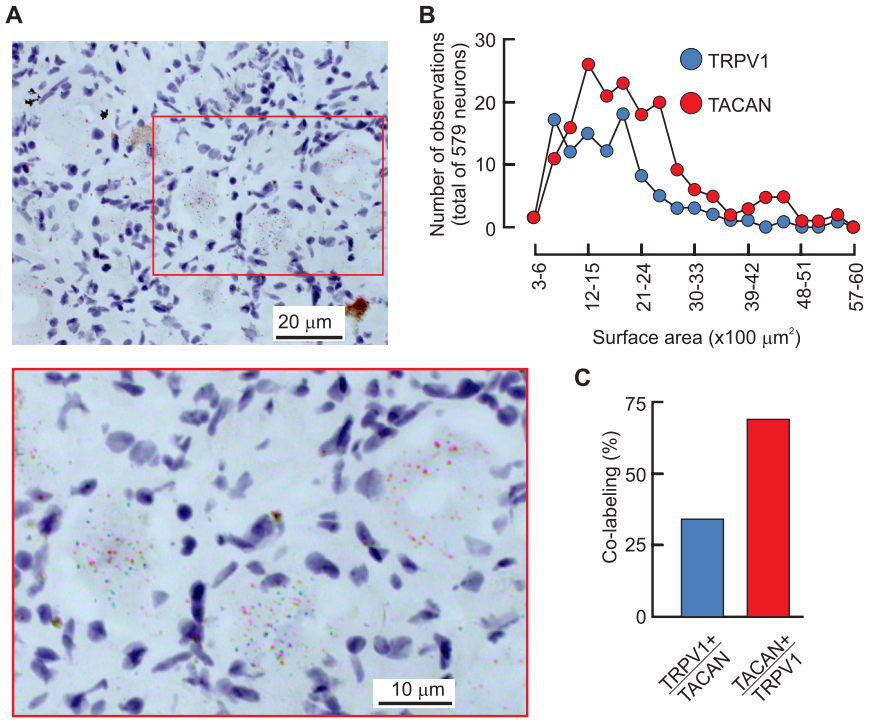

Figure S1. TACAN Is Expressed in Human Sensory Neurons, Related to Figure 2

(A) *In situ* hybridization examining the presence of TACAN in human DRG sections. Bottom panel is a magnification of the box in upper panel, with the TACAN probe in red and the TRPV1 probe (a marker of nociceptive neurons) in blue.

(B) Cross-sectional area distribution of TACAN and TRPV1 mRNA-positive neurons.

(C) Percentage of TRPV1 mRNA-positive neurons that express TACAN mRNA (blue), and percentage of TACAN mRNA-positive neurons that express TRPV1 (red). A total of 579 neurons were examined.

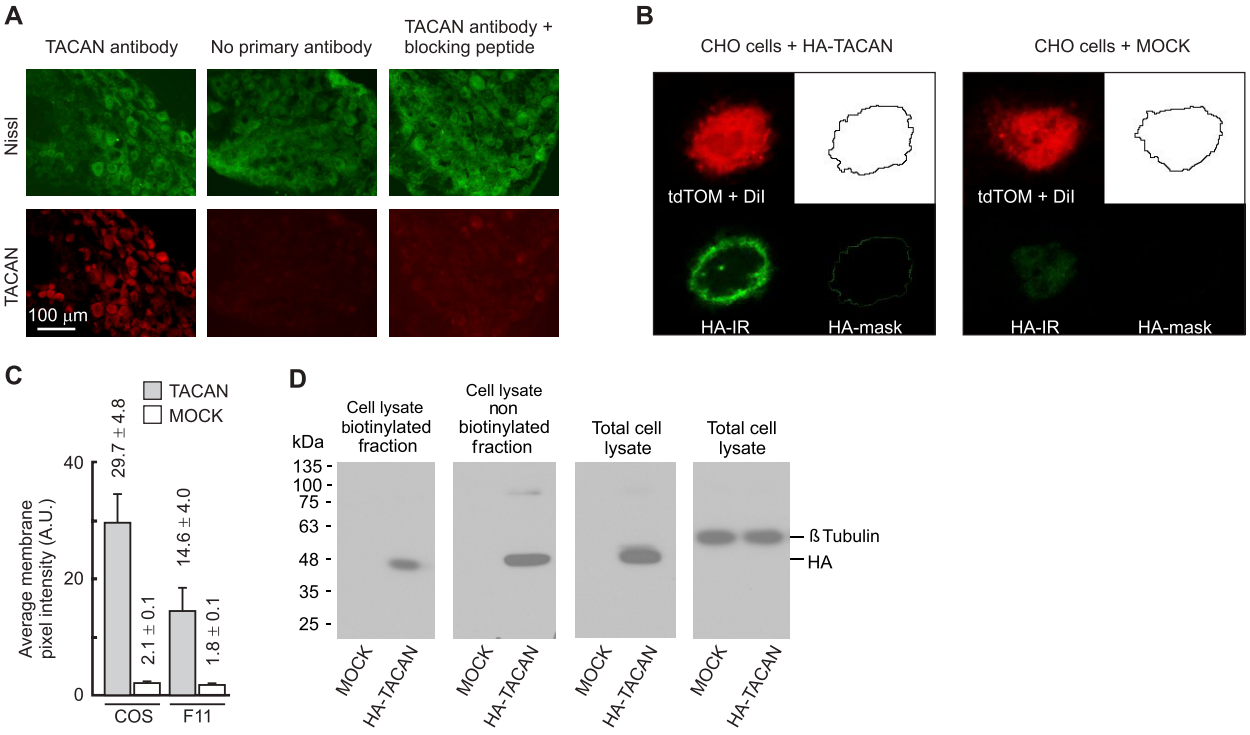

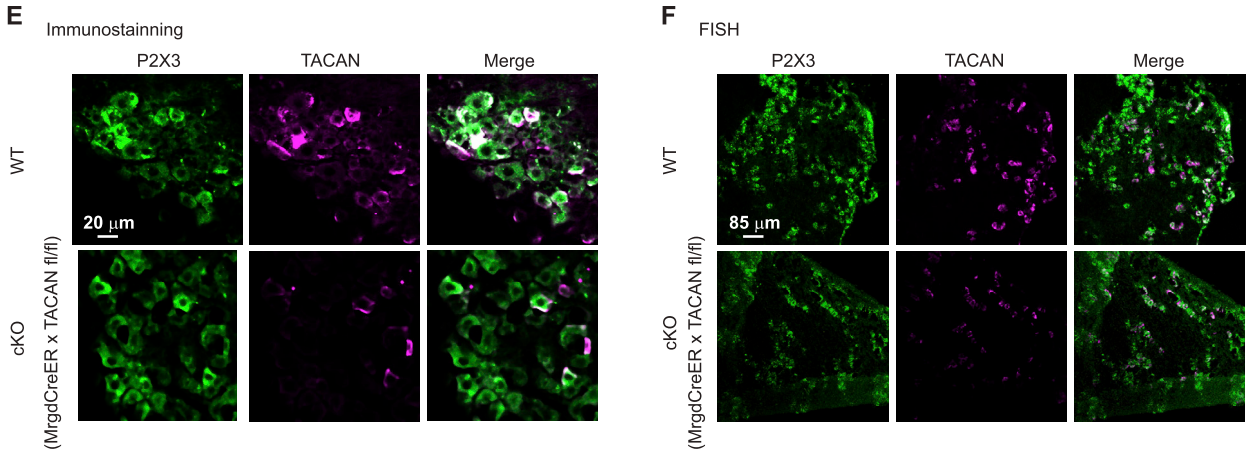

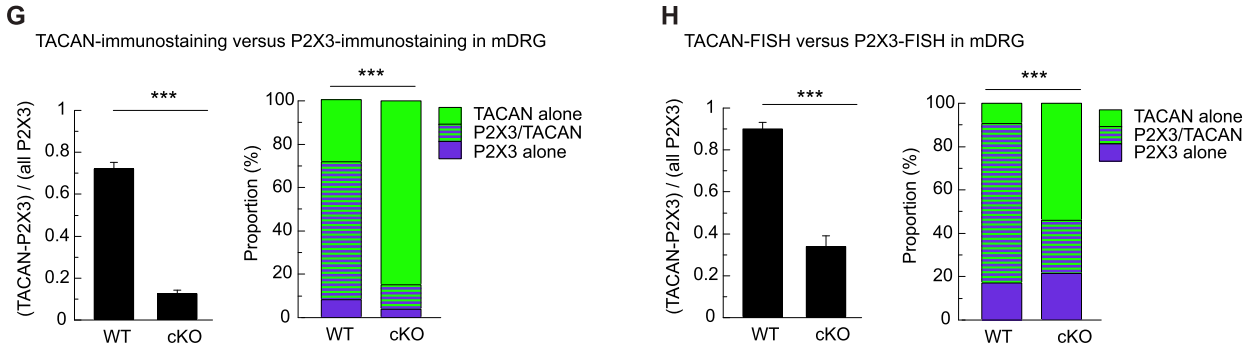

(legend on next page)

Figure S2. Generation of a TACAN Antibody and Cellular Localization, Related to Figure 2

(A) Immunostaining to validate the TACAN antibody (lower panels) along with a background Nissl stain (upper panels). TACAN antibody reveals a subset of immune-positive DRG neurons (left panel). Omission of the primary antibody (middle panel) or its pre-incubation with the antigenic peptide (right panel) demonstrate it is recognizing TACAN.

(B) Membrane staining and imaging of HA-TACAN. Representative images of CHO cells stably expressing HA-TACAN (left set) or the control (MOCK, right set). The signal from extracellular DiI was used to generate a plasma membrane mask (top right panels) which was then applied to the HA signal (HA-TACAN fusion).

(C) Mean (±s.e.m.) membrane pixel intensity from the analysis described in B.

(D) Membrane biotinylation of HA-TACAN stably-transfected CHO cells. First panel (from left): plasma membrane-biotinylated HA-TACAN. Second panel: Non-biotinylated cell lysates indicating the intracellular HA-TACAN. Third panel: Total cell lysate showing TACAN expression. Fourth panel: Total cell lysate showing equal protein loading (beta-tubulin).

(E) P2X3 immunoreactivity (P2X3-IR, left), TACAN-IR (middle) and merge image (right) in wild-type (WT) and Mrgd-creER x TACANfl/fl mice treated with tamoxifen (cKO).

(F) Same as E but with mRNA expression (FISH).

(G) Left, quantification for E. The percentage of WT P2X3-IR neurons that colocalizes with the TACAN-IR is 71.99 ± 0.03% (n = 220/317) in WT and 12.39 ± 0.02% (n = 40/344) in cKO. Right, proportion of neurons exhibit P2X3-IR, TACAN-IR or both in WT and cKO mice.

(H) Left, quantification for F. The percentage of WT P2X3 mRNA neurons that colocalizes with the TACAN mRNA is 90.32 ± 0.02% (n = 279/314) in WT and 33.75 ± 0.05% (n = 70/225) in cKO. Right, proportion of neurons exhibit P2X3 mRNA, TACAN mRNA or both in WT and cKO mice.

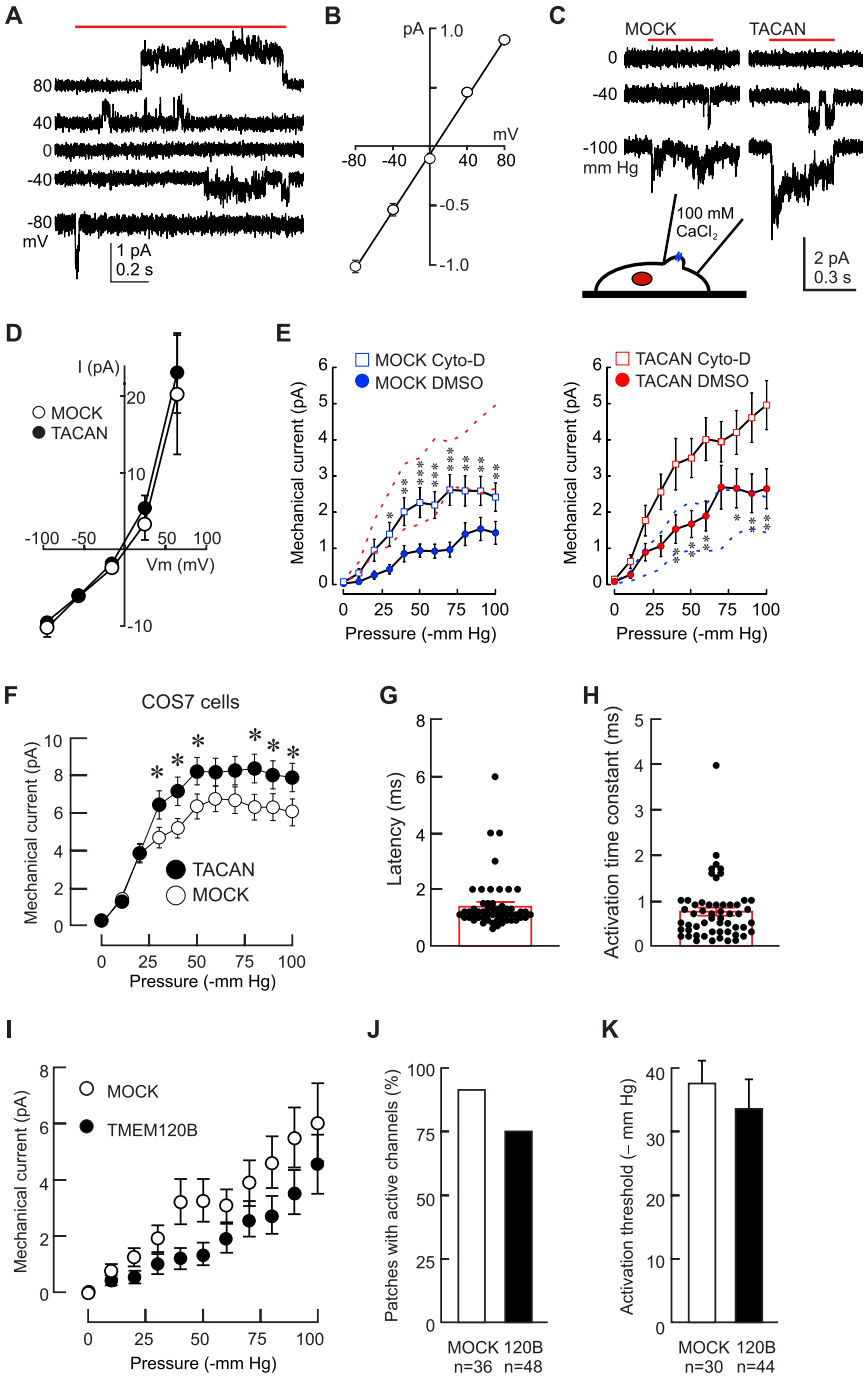

Figure S3. Characterization of TACAN in Heterologous Systems, Related to Figure 3

(A) Representative single-channel currents in HA-TACAN stable CHO cells elicited by mechanical stimuli (red bar) while holding the membrane at different voltages.

(B) Mean (±s.e.m.) single-channel currents extracted from A (n = 11).

(C) Cell-attached single-channel recordings from MOCK- and TACAN-expressing CHO cells with 100mM $CaCl_2$ as the only charge carrier to examine whether the channel can flux Ca^{2+} ions. Red lines indicate when the negative pressure pulse was applied.

(D) Mean (±s.e.m.) whole-cell current-voltage relation of stable CHO cells expressing HA-TACAN or MOCK.

(E) F-actin modulation of mechanically-evoked currents. MOCK- (left panel) or TACAN- (right panel) expressing CHO cells incubated with DMSO (n = 57 and 60 in MOCK- and TACAN-expressing cells, respectively) or cytochalasin D (Cyto-D, 1μM) (n = 48 and 59 for MOCK- and TACAN-expressing cells, respectively). *, **, *** = $p < 0.05$; 0.01; 0.001, respectively. Two-way ANOVA with Tukey post hoc test, comparing DMSO to cytochalasin D.

(legend continued on next page)

(F) Mean (±s.e.m.) mechanically-evoked currents in COS7 cells expressing MOCK (n = 92) or TACAN (n = 100). * = $p < 0.05$; indicate significant difference from MOCK group (Two-way ANOVA with Tukey post hoc test).
(G) Delay between pillar deflection and generation of the whole-cell current in P1KO cells transfected with TACAN. Data are displayed as individual values with the mean (±s.e.m.) superimposed in red.
(H) Activation time constant of mechanically-evoked (pillar deflection) whole cell currents in P1KO cells transfected with TACAN. Data are displayed as individual values with the mean (±s.e.m.) superimposed in red.
(I) Mean (±s.e.m.) mechanically-evoked currents in CHO cells stably expressing MOCK (n = 48) or TMEM120B (n = 36).
(J) Percentage of cell-attached recordings with at least one active MSC. Fisher's Exact Probability test, p = 0.204.
(K) Mean (±s.e.m.) activation threshold of MSCs in CHO cells transfected with MOCK (n = 44) or TMEM120B (n = 30).

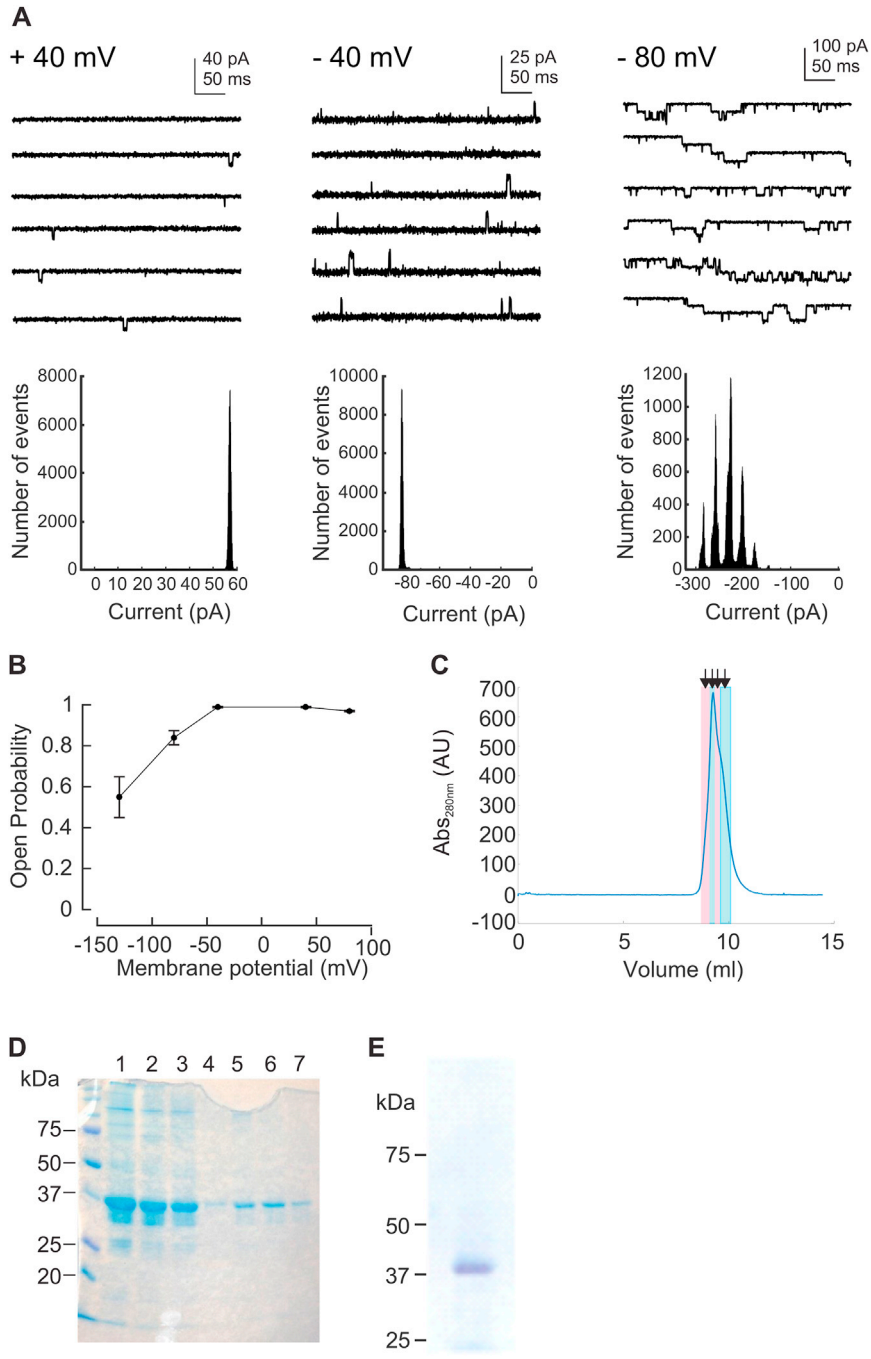

Figure S4. Additional Characterization of TACAN in Lipid Bilayers, Related to Figure 4

(A) Currents elicited by TACAN fused into planar lipid bilayers. Currents were elicited by pulses from 0 mV to the indicated membrane potentials. Each trace represents the zoom onto one pulse. Pulse length was 500 ms with return to 0 mV for 300 ms between pulses. Because of the high open probability and more than one channel per bilayer, the fully closed state is seldom occupied and not shown. Amplitude histograms were obtained from total points histograms. Here, zero current is indicated at 0 pA.

(B) Open probability of TACAN reconstituted in proteoliposomes fused to planar lipid bilayer. Single channel currents were elicited upon pulsing from 0 mV to the indicated membrane potential. Open probability was determined from total point amplitude histograms of the traces. Bilayers were formed of DPhPC.

(C) Size exclusion chromatogram (SEC) profile of TACAN purification. The arrows indicate the fractions shown in gel in D (lanes 4-7).

(D) SDS-PAGE 11% of the fractions from the SEC. Lanes 1-3 are from the earlier purification steps. Lanes 4-7 are fractions of the SEC run shown in C. Lanes 5 & 6 were pooled and used for reconstitution.

(E) SDS-PAGE gel (10% acrylamide) of purified TACAN in Coomassie stain.

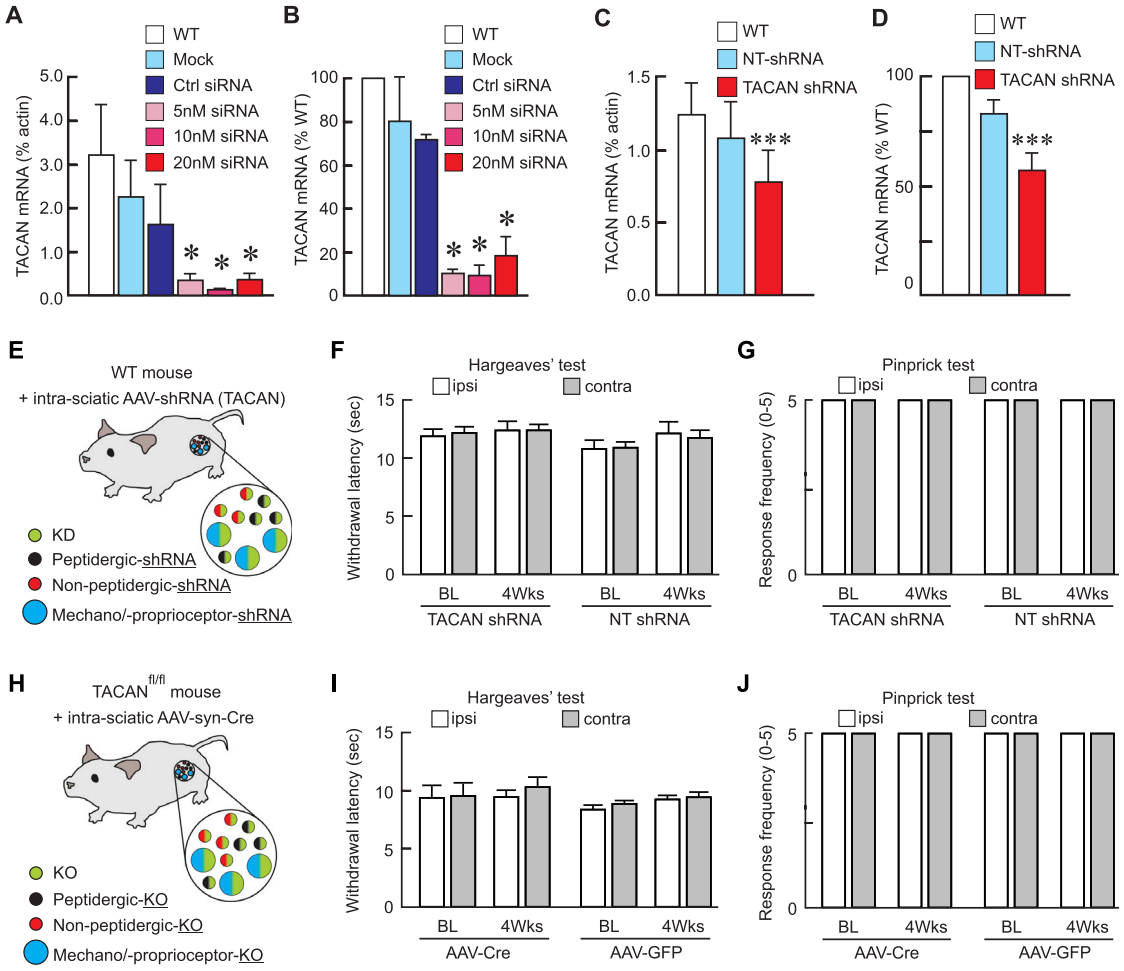

Figure S5. Downregulation of TACAN: mRNA Validation and Effect on Sensitivity to Heat or Pinprick Stimuli, Related to Figure 5

(A) Mean (±s.e.m.) expression level of TACAN, expressed as percent of actin, in non-treated N2A cells (WT), or N2A cells treated with buffers only (MOCK), a non-targeting siRNA (Ctrl), or increasing doses of TACAN-targeting siRNA.

(B) Same data as in A expressed as percentage of the non-treated WT group. * = $p < 0.05$, Kruskal-Wallis One Way ANOVA on Ranks with Dunnett's method, compared to WT group (n = 3 individual experiments, each in quadruplicate).

(C) F11 cells (WT), cells treated with a non-targeting shRNA (NT), or a TACAN-targeting shRNA.

(D) Same data as in C expressed as percentage of the non-treated group. *** = $p < 0.001$ Kruskal-Wallis One Way ANOVA on Ranks with Dunnett's method, compared to the WT group. (n = 3 individual experiments, each in quadruplicate).

(E) Schema of the TACAN knockdown strategy, using WT mice that received an intra-sciatic injection of an AAV2/6 carrying a shRNA against TACAN (n = 13) or a non-targeting control (n = 12).

(F) The broad range reduction in TACAN expression in DRG neurons does not affect sensitivity to heat. Mean (±s.e.m.) withdrawal latencies in the Hargreaves radiant heat test.

(G) The same approach also failed to change the sensitivity to the pin prick test. Frequency of paw withdrawal in response to 5 applications of a pinprick stimulus. Groups are the same as in B.

(H–J) Similar tests as in E-G, except that the assays were run on TACAN$^{fl/fl}$ mice that received a Cre- (n = 5) or GFP- (n = 6) expressing virus.

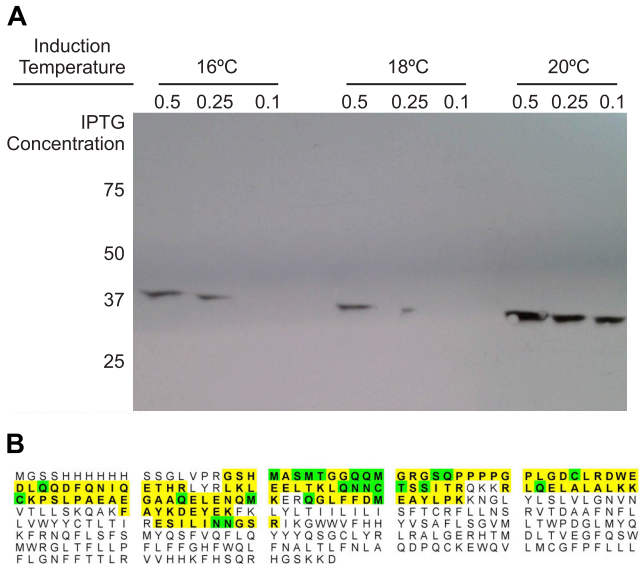

Figure S6. Expression of TACAN in *E. coli* and TACAN Sequence Used for Mass Spectrometry, Related to STAR Methods

(A) Expression was optimal at 20°C and an IPTG concentration of 0.5mM. TACAN was detected at ~37kDa using anti-His antibodies.

(B) TACAN was identified for mass spectrometry by 130/376 amino acids (35% coverage). Yellow and green show amino acids identified in the mass spectrometry. Green identifies amino acids with posttranslational modifications.